UNIFIED MODEL FOR PSEUDO-SLUG AND CHURN FLOWS

by

Mohammad Aljasser

Copyright by Mohammad Aljasser, 2022

All Rights Reserved

A thesis submitted to the Faculty and the Board of Trustees of the Colorado School of Mines in partial fulfilment of the requirements for the degree of Master of Science (Petroleum Engineering).

Golden, Colorado

Date_____

Signed: _____
Mohammad Aljasser

Signed: _____
Dr. Yilin Fan
Thesis Advisor

Golden, Colorado

Date_____

Signed: _____
Dr. Jennifer L. Miskimins
Professor and Head
Department of Petroleum Engineering

ABSTRACT

Multiphase flow is a term used to express a flow that deals with two or more immiscible phases. In the oil and gas production system, multiphase flow can occur in the wellbore and pipelines, and gas-liquid two-phase flow is one of the most common ones. The term flow pattern describes the distribution of each phase in the multiphase flow system. The major flow patterns in gas-liquid two-phase flow include segregated flow, intermittent flow, bubbly flow and dispersed bubble flow. Intermittent flow is one of the most common flow patterns that occurs in the oil and gas wellbore and pipeline system. For horizontal or inclined pipes, intermittent flow can be further classified into plug flow, slug flow, and pseudo-slug flow. For vertical or near vertical pipe, intermittent flow can be classified into slug flow and churn flow. The focus of this study will be on the two least studied flow patterns namely pseudo-slug and churn flows.

Pseudo-slug and churn flows are generally considered as two different flow patterns because of their visual differences. However, some recent experimental studies have shown that they share many similarities. For example, they both have gas penetration through the slug body; they both locate between slug and segregated flow in the flow pattern map; they demonstrate similar time trace signals of liquid holdup equivalent and distribution histogram; their structure velocities are smaller than the one for conventional slug flow. According to the observation from previous experimental studies, we anticipate that pseudo-slug flow gradually changes to churn flow when the inclination angle changes from horizontal to vertical.

In this study, we developed a simplified unified hydraulic model for pseudo-slug and churn flows, that captures the effects of inclination angle, gas and liquid flow rates, and fluid properties, such as liquid viscosity and gas density, on the liquid holdup and pressure gradient. It removes the need for the user to switch the models as the flow pattern (or inclination angle)

changes. The liquid holdup is predicted using the drift-flux model concept, with new correlations for the drift velocity and flow distribution coefficient. The pressure gradient is predicted using two-fluid model with modified gas and liquid shear stresses by considering the additional shear induced by the “huge wave” structures and the oscillated nature of the liquid film caused by gravity. The model gives the best predictions as compared with other available models in the literature, in terms of predictions for pseudo-slug flow solely, churn flow solely, and both flow patterns.

TABLE OF CONTENTS

LIST OF FIGURES

LIST OF TABLES

NOMENCLATURE

English Letters

Symbol	Description	Units
A_G	Gas occupied cross-sectional area	m^2
A_L	Liquid film occupied cross-sectional area	m^2
A_P	Pipe cross-sectional area	m^2
C_0	Drift-flux flow distribution coefficient	-
C_{0HR}	Distribution coefficient for high Reynolds number	-
d	Pipe inner diameter	m
dp/dL	Total pressure gradient	Pa/m
e_{ri}	Relative error	-
f_G	Gas wall friction factor	-
f_{G_SP}	Single phase gas wall friction factor	-
f_{GM}	Modified gas wall friction factor	-
f_I	Interfacial friction factor	-
f_L	Liquid wall friction factor	-
g	Gravitational acceleration	m/s^2
h_L	Liquid film thickness	m
H_L	Total liquid holdup	-
H_{Lcr}	Critical liquid holdup	-
Re_{TP}	Mixture Reynolds number	-
S_G	Gas wetted perimeter	m
S_I	Interfacial perimeter	m
S_L	Liquid wetted perimeter	m
S_{L_FI}	Liquid wetted perimeter for flat interface	m
v_D	Drift velocity	m/s
v_G	Average gas phase velocity	m/s
v_L	Average liquid film velocity	m/s
v_M	Mixture velocity	m/s

v_{SG}	Gas superficial velocity	m/s
v_{SL}	Liquid superficial velocity	m/s

Greek Letters

Symbol	Description	Units
α	Gas void fraction	-
ε_2	Absolute average relative error	%
μ_G	Gas dynamic viscosity	Pa.s
μ_L	Liquid dynamic viscosity	Pa.s
ρ_g	Gas density	kg/m^3
ρ_L	Liquid density	kg/m^3
ρ_M	Mixture density	kg/m^3
σ	Surface tension	N/m
τ_{WG}	Average gas wall shear stress	Pa
τ_{WL}	Average liquid wall shear stress	Pa
τ_i	Interfacial shear stress	Pa
θ	Inclination angle from horizontal	°

CHAPTER 1
INTRODUCTION

Multiphase flow is a term used to express a flow that deals with two or more immiscible phases. In the oil and gas production system, multiphase flow can occur in the wellbore and pipelines, and gas-liquid two-phase flow is one of the most common ones. The term flow pattern describes the distribution of each phase in the multiphase flow system. Each flow pattern occurs in certain values of different variables that control the flow behaviors. These variables can be classified into three major categories, operational parameters (i.e., flow rates), geometrical parameters (i.e., pipe diameter and inclination), and the physical properties of the phases (i.e., density, viscosity, and surface tension). For gas-liquid two-phase flow in pipes or wellbores, major flow patterns include segregated flow (SEG), intermittent flow (INT), bubbly (BL, only for vertical or near vertical), and dispersed bubble flow (DB). Segregated flow includes stratified flow (ST) which occurs at horizontal or inclined pipes, and annular flow (AN) that occurs at high gas flow rate conditions and at any pipe inclinations. Dispersed bubble flow occurs at high liquid flow rates and low gas flow rates at any pipe inclinations, and bubbly flow is only observed in vertical or near vertical pipes at low gas flow rate conditions. Intermittent flow is one of the most common flow patterns that occurs in the oil and gas wellbore and pipeline system (Shoham 2006). For horizontal or inclined pipes, intermittent flow can be further classified into plug flow (PL), slug flow (SL), and pseudo-slug flow (PS). For vertical or near vertical pipe, intermittent flow can be classified into slug flow and churn flow (CH). The focus of this study will be on the two least studied flow patterns, namely pseudo-slug and churn flows.

Pseudo-slug flow is considered as a transition flow pattern between conventional slug and segregated flows as the superficial gas velocity increases. It mainly occurs in horizontal or

upward inclined pipes. The pseudo-slug flow can be differentiated from the slug flow by having a slug body that does not completely seal the cross-sectional area of the pipe, unlike the conventional slug flow pattern. Churn flow mainly occurs in vertical or near-vertical pipes, and is considered as one of the least investigated flow patterns due to the complexity of its nature. Similar to slug flow, gas pockets flow along with the liquid phase in churn flow but in a more chaotic way. In churn flow, the bullet-shaped Taylor bubbles, a structure that shows a clear bullet-shaped interface on top and occurs typically in conventional slug flow, are distorted because of the relatively higher gas flow rates causing asymmetrical random gas pockets.

Pseudo-slug and churn flows are generally considered as two different flow patterns because of their visual differences. However, some recent experimental studies have shown that they share many similarities (Parsi et al. 2017; Soedarmo et al. 2018c). For example, they both have gas penetration through the slug body; they both locate between slug and segregated flow in the flow pattern map; they demonstrate similar time trace signals of liquid holdup equivalent and distribution histogram; their structure velocities are smaller than the one for conventional slug flow; their drift-flux distribution coefficients fall in a similar range; and the use of slug flow model results in significant discrepancies in pressure gradient and liquid holdup predictions for both flow patterns. According to the observation from previous experimental studies, we anticipate that pseudo-slug flow gradually changes to churn flow when the inclination angle changes from horizontal to vertical.

Highly inclined pipelines have become common especially in unconventional applications, and the wellbore can range from horizontal to vertical with the current advancement in directional drilling. Accurate prediction of the pressure gradient and liquid holdup will be of great importance to the production design. There are several hydraulic models available in the

literature for churn flow, while the modeling for pseudo-slug flow has just emerged in recent years (Soedarmo et al. 2018c). Some of the models predict well for pseudo-slug flow but poorly for churn flow, and vice versa. There is no single model that works well for both pseudo-slug and churn flows. With the current modeling approaches, the user needs to switch the model from pseudo-slug to churn flow when the inclination angle increases from inclined to near vertical to obtain more accurate predictions in liquid holdup and pressure gradient. However, the critical inclination angle corresponding to this flow pattern transition can be gradual and depends on the flowing conditions (such as liquid flow rate, diameter, and fluid properties), and is still not clear. Switching the model will also result in discontinuity in model prediction which can lead to problems when coupled with reservoir simulations or uncertainties in facility and production design. In addition, evaluation of these existing models still shows unsatisfactory predictions although they are developed for the targeted flow pattern.

In this study, we developed a simplified unified hydraulic model for pseudo-slug and churn flows, that captures the effects of inclination angle, gas and liquid flow rates, and fluid properties, such as liquid viscosity and gas density, on the liquid holdup and pressure gradient. It removes the need for the user to switch the models as the flow pattern (or inclination angle) changes. The liquid holdup is predicted using the drift-flux model concept, with new correlations for the drift velocity and flow distribution coefficient. The pressure gradient is predicted using two-fluid model with modified gas and liquid shear stresses by considering the additional shear induced by the "huge wave" structures and the oscillated nature of the liquid film caused by gravity. The model gives the best predictions as compared with other available models in the literature, in terms of predictions for pseudo-slug flow solely, churn flow solely, and both flow patterns.

CHAPTER 2
LITERATURE REVIEW

This chapter provides a literature review on the experimental studies on pseudo-slug and churn flows, followed by the modeling studies.

2.1 Review of Pseudo-slug and Churn Flows

This section introduces pseudo-slug and churn flows, followed by a discussion on their similarities.

2.1.1 Introduction to Pseudo-slug Flow

Pseudo-slug flow is generally characterized by short, undeveloped, frothy chaotic slugs. It occurs at the transition between the conventional slug and segregated flows, while the location in a flow pattern map depends on the pipe inclination angle (Fan et al. 2020). It mainly occurs in horizontal or upward inclined pipes. The pseudo-slug flow can be differentiated from the slug flow by having a slug body that does not completely seal the cross-sectional area of the pipe unlike the conventional slug flow pattern as illustrated in Figures 2-1 and 2-2.

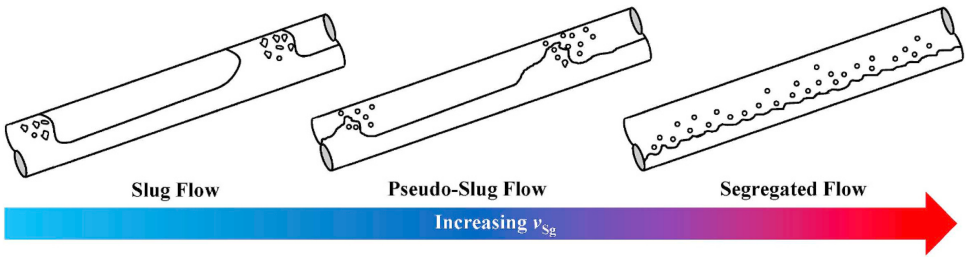

Figure 2-1 PS illustration in slightly upward inclined flow (Soedarmo et al. 2018a).

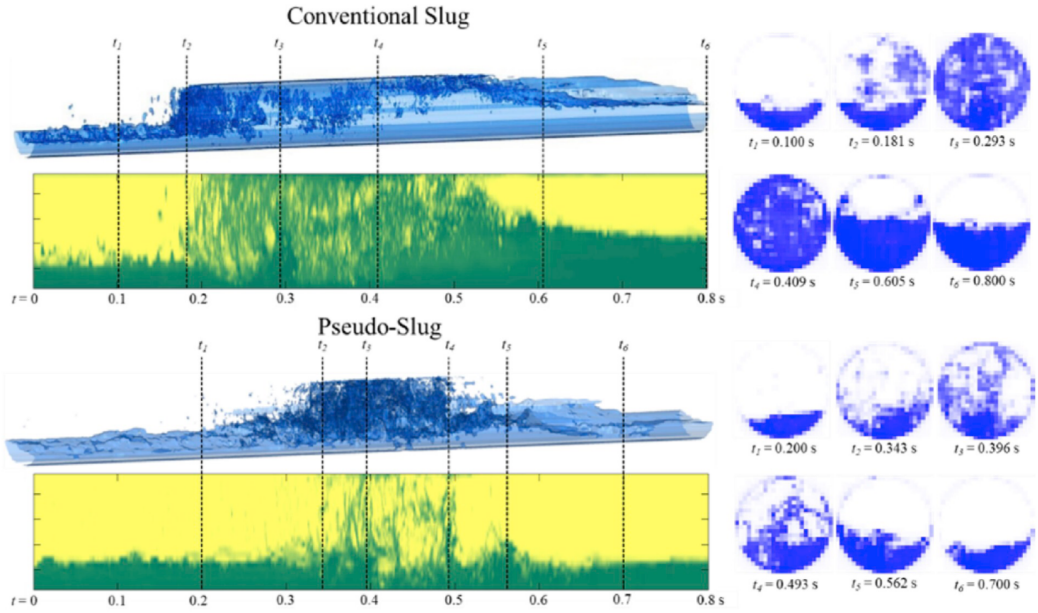

Figure 2-2 PS vs SL flow wire-mesh sensor visualization (Fan et al. 2020).

Lin and Hanratty (1987) identified pseudo-slugs as disturbances that have the appearance of slugs but do not give the identifying pressure pattern and do not travel at the gas velocity (Lin and Hanratty 1987). It resembles annular flow when a continuous liquid film is formed on the pipe circumference, wavy-stratified flow when a thick layer of liquid is present at the bottom of the pipe, and slug flow when large slug-like structures are capable of reaching the top of the pipe are present.

Due to its ambiguous flow characteristics, this type of flow has been identified with different literature names, even until today. Nicholson et al. (1978) used "proto-slug" to describe the "unstable wave-like events which are not quite able to bridge the pipe cross-section," which was adopted by some other studies, such as (Bendiksen and Espedal 1992), and (Kokal and Stanislav 1989). Kokal and Stanislav (1989) also called it a "proto-slug froth" flow regime, while Abduvayt et al. (2003) designated it as "froth" flow. This structure was reported by Hunt et al.

(2004) under the Norwegian colloquial name as a "ghost," a name that referred to its character as it passed at high speed along the pipe with a sort of whispering noise, which was equivalent to the "huge wave" observed by Sekoguchi and Mori (1997) and Hunt and Millington (2016). Some researchers named it as a wave structure, such as "roll-waves" (Soleimani et al. 2002), "large amplitude roll-waves" (De Leebeeck 2010), and "disturbance waves" (Butterworth and Pulling 1972; Taylor et al. 2014). Furthermore, some studies treated it as a sub-regime of other well-established flow patterns, such as "Annular Flow"/"Wavy Annular" (Taitel and Dukler 1976; Barnea et al. 1980; Shoham 2006), "High-aerated slugs" or "Slug and Wavy" (Vaze and Banerjee 2011; Thaker and Banerjee 2015; Arabi et al. 2020). In recent years, some researchers used "Gas-Core Slugs" to describe the slug structures that had a gas-core based on ECT (Electrical Capacitance Tomography) measurement (Hunt and Millington 2016; Arellano et al. 2020). Lin and Hanratty (1987) provided a detailed description of this flow pattern and presented flow pattern maps for horizontal pipe flow with two diameters. They called this flow pattern as "pseudo-slug" flow, which is widely adopted by the studies afterward (Wilkens and Jepson 1996; Maley 1997; Soleimani et al. 2002; Langsholt and Holm 2007; Alsaadi et al. 2015; Lam Loh et al. 2016; Kesana et al. 2017; Parsi et al. 2017; Soedarmo et al. 2018c; Fan et al. 2020).

Previously, pseudo-slug had been thought to occupy a narrow range on the classic flow pattern map. However, recent studies show that pseudo-slug flow can occupy a wider range on the flow pattern map, especially in some specific cases such as large wellbores with low liquid flow rates, large diameter gas condensate pipelines, and pipes with high inclination angles (Fan et al. 2020). As for the inclination angle of the pipe, Figure 2-3 shows the effects of inclination angle and superficial liquid velocity on the area occupied by pseudo-slug flow. It shows that as

the inclination angle increases from 2° to 20°, the pseudo-slug flow region expands. It also shows that the pseudo-slug flow region expands as the superficial liquid velocity increases from 0.005 to 0.01 m/s. Previous studies also show that the area occupied by pseudo-slug flow expands with increasing pipe diameter, reducing pressure, and increasing liquid viscosity (Alsaadi 2013, 2019; Ekinci 2015; Rodrigues 2018).

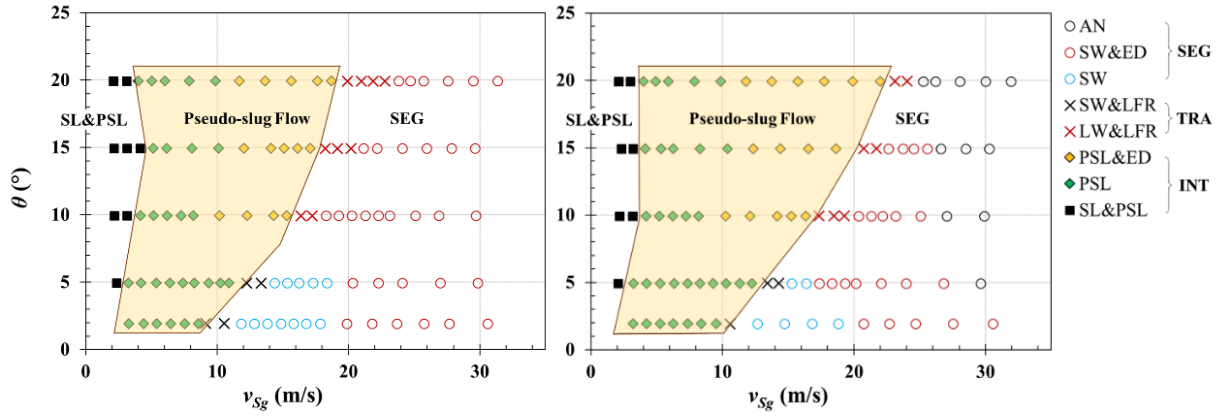

Figure 2-3 Area occupied by PS flow in flow pattern map (left: v_{SL} = 0.005 m/s; right: v_{SL} = 0.01 m/s) (Fan et al. 2020).

2.1.2 Introduction to Churn Flow

For vertical pipe flow, churn flow is considered as one of the least investigated flow patterns due to the complexity of its nature. Figure 2-4 shows a typical flow pattern map for gas-liquid flow in a vertical pipe (Collignon et al. 2018). Churn flow commonly occurs between the slug and annular flows.

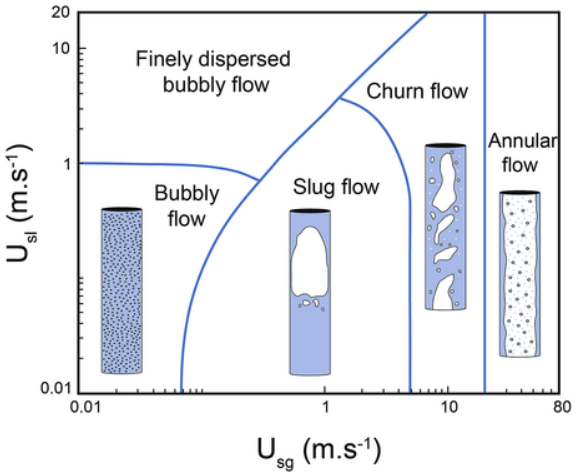

Figure 2-4 Flow pattern map for gas-liquid flow in a vertical 72-mm pipe (Collignon et al. 2018).

Similar to slug flow, gas pockets flow along with the liquid phase in churn flow but in a more chaotic way (Figure 2-5). In churn flow, bullet-shaped Taylor bubbles are distorted because of the relatively higher gas flow rates causing asymmetrical random gas pockets (Sekoguchi and Mori 1997). It occurs mainly in vertical and near-vertical pipes. There are three "liquid lumps" in churn flow as Sekoguchi and Mori (1997) observed in their study, namely slugs, huge waves, and disturbance waves. Slugs are liquid lumps that move with an almost constant velocity covering the whole cross-sectional area of the pipe. Huge waves referred by other researchers as "flooding-type waves" are large liquid waves flowing upward due to the force exerted by the gas phase with a gas core in the middle. Disturbance waves differ from huge waves by having thinner liquid film, and are dominated in annular flow (Dasgupta et al. 2017).

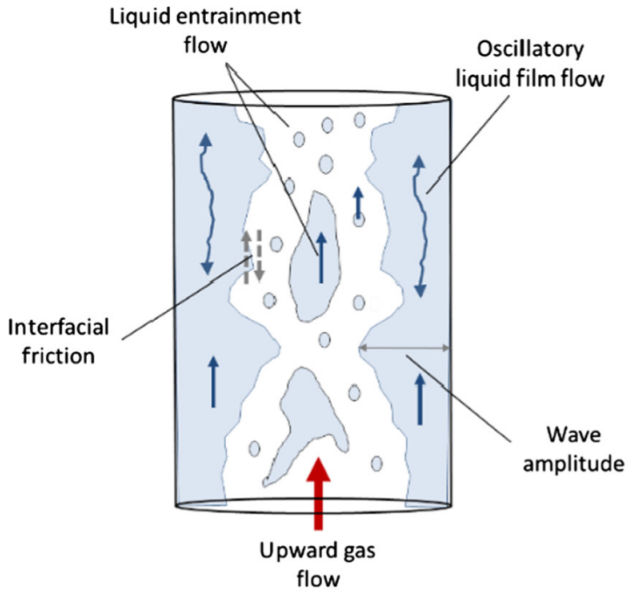

Figure 2-5 Schematic of churn flow (Pagan et al. 2017).

Some studies show that churn flow observed in larger-diameter pipes has a wider range of gas-liquid ratios than smaller pipe diameters (Omebere-Iyari and Azzopardi 2007). Zabaras et al. (2013) showed that churn flow was observed in a larger diameter pipe at the same flowing condition where slug flow should be observed in smaller diameter pipes.

2.1.3 Similarities Between Pseudo-slug and Churn Flows

Pseudo-slug and churn flows are commonly considered as two different flow patterns mainly because of their visual differences. Parsi et al. (2017) and Soedarmo et al. (2018c) provided a detailed discussion about the similarities and differences between pseudo-slug and churn flows. In summary, the most significant differences between PS and CH are that CH does not exhibit easily distinguishable film and slug regions from a visualization point of view, and the liquid phase distribution for CH is more uniform surrounding pipe wall than PS due to

gravity effects. On the other hand, PS has demonstrated more similarities with CH, which can be summarized in the following six points.

1. Flow visualization: Both PS and CH have gas penetration through the liquid structure, as illustrated in Figure 2-6.

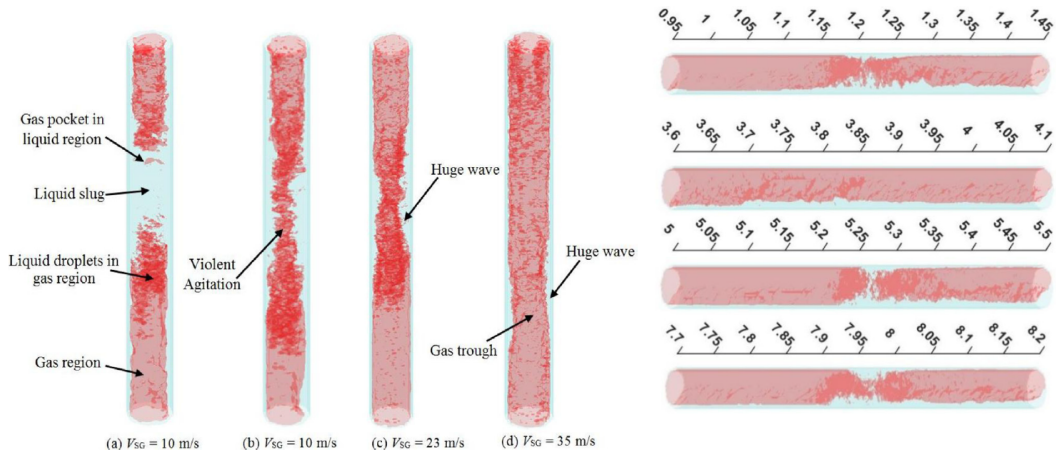

(a). Vertical upward (CH in c &d) (v_{SL} = 0.76 m/s; v_{Sg} = 10, 23, 35 m/s θ = 90°; d = 76.2 mm)

(b) Horizontal (v_{SL} = 0.76 m/s; v_{Sg} = 17.7 m/s; θ = 0°; d = 76.2 mm)

Figure 2-6 3-D iso-void fraction images from wire-mesh sensor (Parsi et al. 2017). (The first two images in (a) correspond to a flow pattern when a conventional slug and churn structure co-exist at the same flowing condition; while the last two in (a) show two churn structures at a higher gas velocity).

2. Location in the flow pattern map: Both flow patterns exist between SL and SEG. High speed camera footage shows that PS flow pattern was observed at near-horizontal and inclined pipes and CH flow pattern was observed at near-vertical pipes (Figure 2-7).

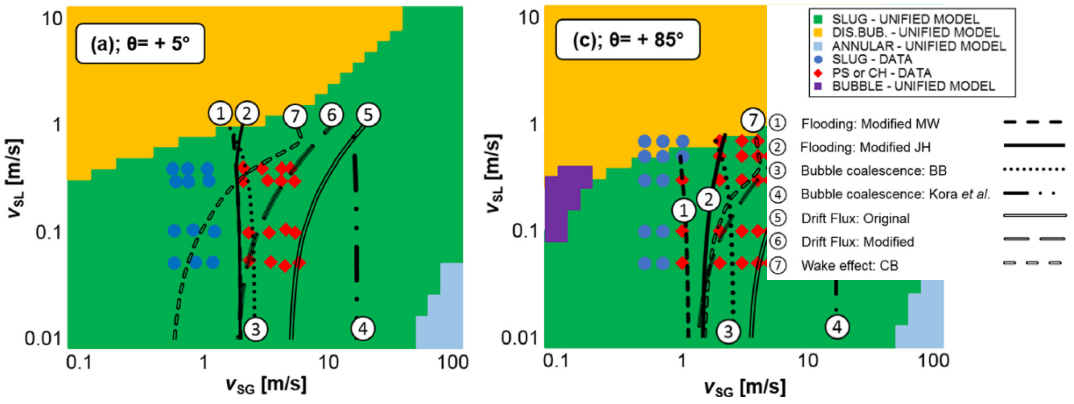

Figure 2-7 Flow pattern for different inclination angles (Soedarmo et al. 2018c).

3. Dimensionless voltage (V') histograms: They display similar behavior in the time trace of liquid holdup equivalent signals and its distribution histogram (Figure 2-8). The histogram of PS and CH normally shows a single peak, while it has two peaks for SL flow representing film and slug body regions respectively.

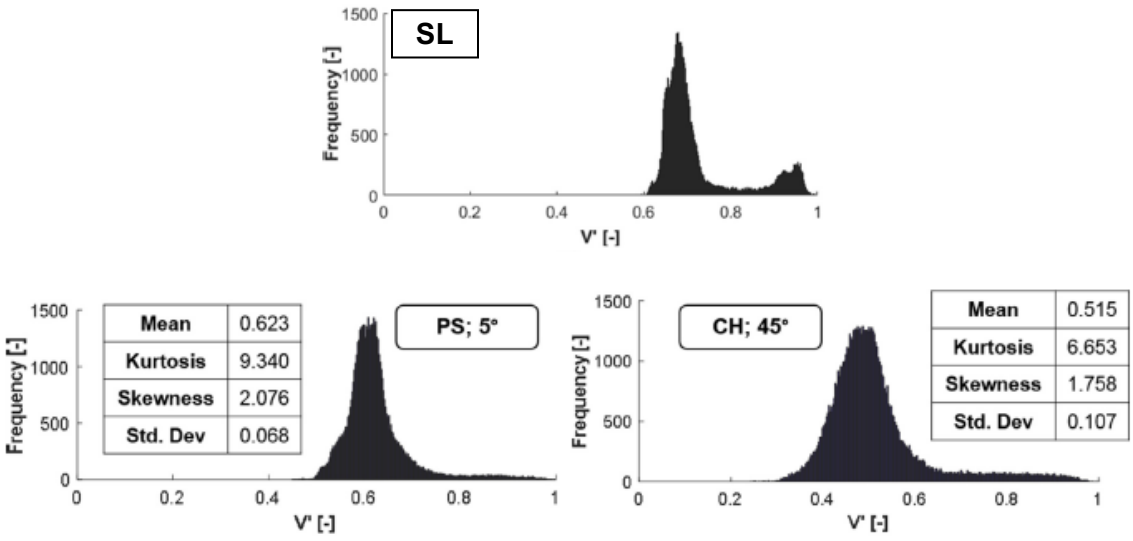

Figure 2-8 Histogram of dimensionless voltage time-trace from capacitance probes for SL, PS, and CH (Soedarmo et al. 2018c).

4. Translational velocity (v_T) behaviors: The translational velocity represents the velocity of the interface between the gas and the liquid at the front of SL, PS, and CH slug/wave body. The relationship between v_T and v_M in conventional SL flow forms a linear relationship. However, PS and CH both have v_T values lower than v_T expected for SL flow, and v_T vs. v_M will no longer have a linear relationship due to the continuous flow of the gas phase that lowers the value of v_T as shown in Figure 2-9.

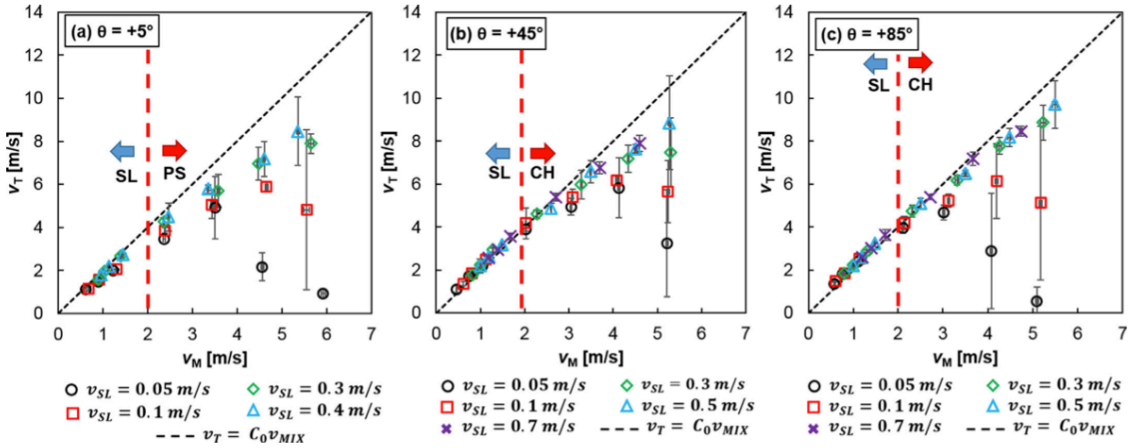

Figure 2-9 v_T vs v_M for SL, PS and CH flows (Soedarmo et al. 2018c).

5. Drift flux flow coefficients (C_0): Distribution coefficient C_0 physically describes the distribution of gas in the flow (Parsi et al. 2017). C_0 for PS and CH flow patterns are within a similar range and smaller than that for conventional SL flows according to previous studies (Parsi et al. 2017; Soedarmo et al. 2018c). Figure 2-10 shows the C_0 that was back-calculated from experimental liquid holdup from Soedarmo et al. (2018c) for high viscosity oil and gas flows (Soedarmo et al. 2018c). The scattering in SL flow region is mainly due to the uncertainties in v_D values.

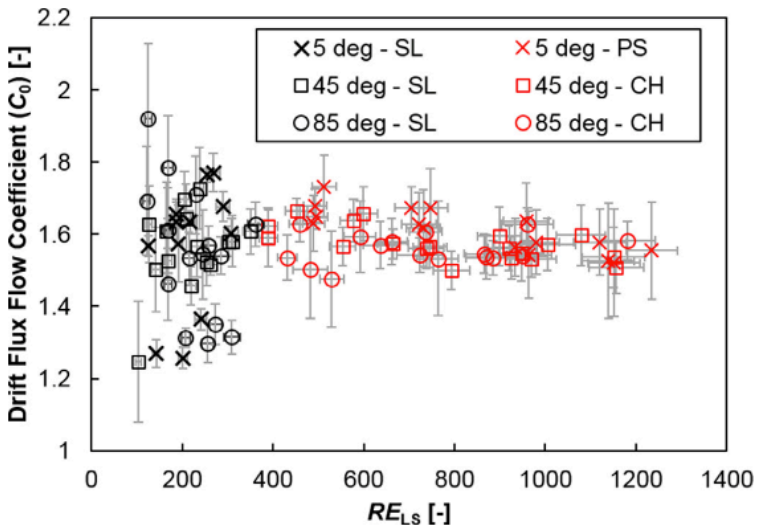

Figure 2-10 C_0 vs Reynolds number (Soedarmo et al. 2018c).

6. Prediction using models developed for conventional SL flows: Using the SL flow model can result in significant discrepancies in pressure gradient predictions (Figure 2-11).

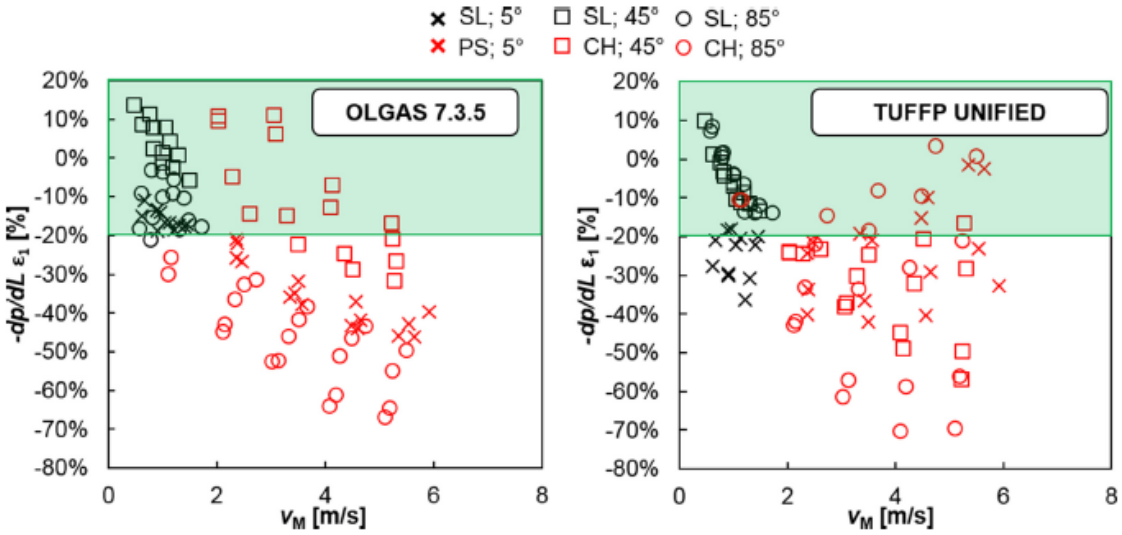

Figure 2-11 Comparison with model predictions (Soedarmo et al. 2018c).

2.2 Previous Modeling Studies on Pseudo-slug and Churn Flows

This section introduces the previous modeling work on churn and pseudo-slug flow respectively.

2.2.1 Previous Modeling Studies on Churn Flow

The previous hydraulic models for churn flow can be classified into three categories, namely modified slug flow model or unit cell model, drift-flux model, and modified segregated flow model. This section introduces the concept respectively for each category.

2.2.1.1 Modified Slug Flow Model for Churn Flow

Tengesdal et al. (1999) proposed two hydrodynamic models based on the modified slug model (or unit cell slug model) and drift-flux model to predict the liquid holdup and pressure gradient. As for the modified slug flow model, CH flow is assumed to have two separate regions, namely gas pocket and liquid film regions, and modeled by modifying Chokshi (1994) unit-slug model for CH flow. The general liquid mass balance equation for a slug unit moving at v_{TBf} (translational velocity) is expressed as:

$$v_{SL} = v_{TBf}\left(\frac{L_{LS}}{L_{SU}}\right)(1-\alpha_{LS}) + v_{TBf}\left[1-\left(\frac{L_{LS}}{L_{SU}}\right)\right](1-\alpha_{TB}) - \left(v_{TBf}-v_{LLS}\right)(1-\alpha_{LS}) \quad (2\text{-}1)$$

where, v_{TBf} is the Taylor bubble front velocity, L_{LS} is liquid slug length, L_{SU} is slug unit length, α_{LS} is the void fraction in the liquid slug region, α_{TB} is the void fraction in the Taylor bubble region, and v_{LLS} is the liquid velocity in the liquid slug region.

The mixture velocity is expressed as:

$$v_M = v_{LLS}\,(1 - \alpha_{LS}) + v_{gLS}\,\alpha_{LS} \tag{2-2}$$

The following expression shows that the amount of liquid that moves upstream relative to the bubble has the same value as the liquid that is overrun by the liquid slug.

$$(v_{TBf} - v_{LLS})(1 - \alpha_{LS}) = \left(v_{TBf} - v_{LTB}\right)(1 - \alpha_{TB}) \tag{2-3}$$

Four more equations are required to solve the mass and volume balances equations, including the correlations for v_{TBf} (translational velocity), v_{LTB} (liquid velocity in gas pocket region) , v_{GLS} (gas velocity in slug body), and α_{LS} (void fraction in slug body).

The total pressure gradient of the slug unit is given as:

$$\left(\frac{dP}{dL}\right)_{total} = \left(\frac{dP}{dL}\right)_{gravitational} + \left(\frac{dP}{dL}\right)_{frictional} \tag{2-4}$$

$$\left(\frac{dP}{dL}\right)_{total} = \frac{L_{LS}}{L_{SU}}\ \rho_{LS}\ g\ \sin\theta\ + \frac{L_{LS}}{L_{SU}}\ \frac{f_M\ \rho_{LS}\ {v^2}_M}{2d} \tag{2-5}$$

where, ρ_{LS} is the liquid density in the liquid film region, given as:

$$\rho_{LS} = (1 - \alpha_{LS})\,\rho_L + \alpha_{LS}\,\rho_g \tag{2-6}$$

f_M is the Moody friction factor, which is a function of the Reynolds number:

$$N_{{Re}_M} = \frac{\rho_{LS}\ v_M\ d}{\mu_{LS}} \tag{2-7}$$

where, μ_{LS} is the liquid slug viscosity, given as:

$$\mu_{LS} = (1 - \alpha_{LS})\,\mu_L + \alpha_{LS}\,\mu_g \tag{2-8}$$

2.2.1.2 Drift Flux Model

The drift flux model treats the two-phase flow as a mixture. It is considered as an improvement over the homogeneous model and a simplification of the two-fluid model. The

general concept of the drift flux model was first proposed by Zuber and Findlay (1965) and later modified by many researchers, such as Wallis (1969) and Ishii (1977). It models the void fraction as a function of superficial gas velocity, mixture velocity, drift velocity, and flow distribution coefficient. França and Lahey (1992) and Danielson and Fan (2009) have shown that the drift flux model for liquid holdup estimations can be applicable for segregated flow patterns even if it is originally suitable for mixed flow patterns such as bubble flow.

The general equation of the drift flux model is given as follows:

$$\alpha = \frac{v_{SG}}{v_G} = \frac{v_{SG}}{C_0 v_M + v_D} \tag{2-9}$$

where α is the void fraction; v_{SG} is the superficial gas velocity defined as the gas volumetric fraction divided by the pipe cross-sectional area; v_G is the average actual gas velocity, which is the superficial gas velocity divided by the void fraction as expressed in the following equation.

$$v_G = \frac{v_{SG}}{\alpha} \tag{2-10}$$

v_M is the mixture velocity which is the summation of the superficial velocities of both phases. C_0 is the flow distribution coefficient which represents the effect of void fraction and velocity distribution on flow behavior and is expressed mathematically in the following equation:

$$C_0 = \frac{< \alpha\, v_M >}{< \alpha >< v_M >} \tag{2-11}$$

The sign "< >" indicates the pipe cross-sectional averaged value. Figure 2-13 illustrates the cross-sectional averaged concept in a pipe by dividing the cross-section into small grids with a total number of *N*. The cross-sectional averaged void fraction $< \alpha >$, mixture velocity $< v_M >$, and the product of the void fraction and mixture velocity $< \alpha v_M >$ are expressed in Equations 2-12 to 2-14, where *i* refers to the i^{th} grid. In the example shown in Figure 2-13, the void fraction and mixture velocity are maximum at the pipe center and decrease approaching the pipe wall.

The corresponding C_0 is 1.14 according to Equation 2-11. One can also easily find that C_0 should equal one when the void fraction or mixture velocity is uniformly distributed at the pipe cross-section.

$$< \alpha > = \frac{\sum \alpha_i}{N} \tag{2-12}$$

$$< v_M > = \frac{\sum v_{M_i}}{N} \tag{2-13}$$

$$< \alpha v_M > = \frac{\sum (\alpha_i v_{M_i})}{N} \tag{2-14}$$

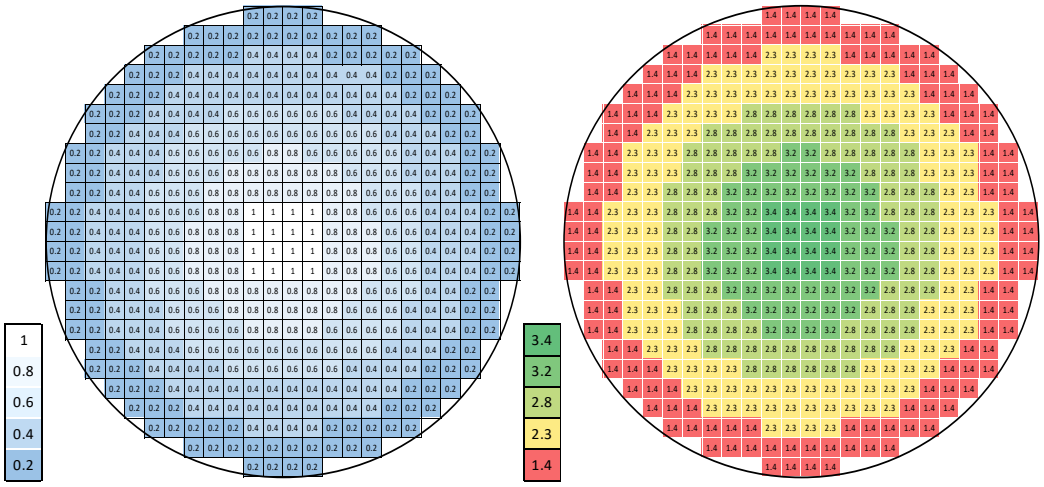

(a) (b)

Figure 2-12 Example to illustrate the average cross-sectional view of multiphase flow in a pipe (a) void fraction values (b) mixture velocity values. The corresponding flow coefficient is 1.14.

v_D in Equation 2-9 which represents the velocity of the gas phase in a stagnant liquid column is the void fraction weighted cross sectional area averaged drift velocity indicated by the sign "<< >>". The numerical expression for v_D in Equation 2-9 is given by:

$$<< v_D >> = \frac{< \alpha\, v_D >}{< \alpha >} \tag{2-15}$$

The value of C_0 depends on the void and velocity distribution in the pipe. Zuber and Findlay (1965) used a hypothetical fluid flow model in a pipe and proved that C_0 equaled to one if the concentration was uniform (i.e., void fraction in the center, α_c, equaled to the void fraction next to the pipe wall, α_w), greater than one if α_c is greater than α_w, and less than one if α_c is lower than α_w. They also illustrated how the void and velocity distribution impact the flow distribution coefficient as illustrated in Figure 2-14. A more pointed velocity or void fraction distribution (such as conditions I and II) results in a higher C_0 compared to the case with a more flat distribution (condition III). The higher the difference between the void fraction at the pipe center and the pipe wall, the higher the C_0.

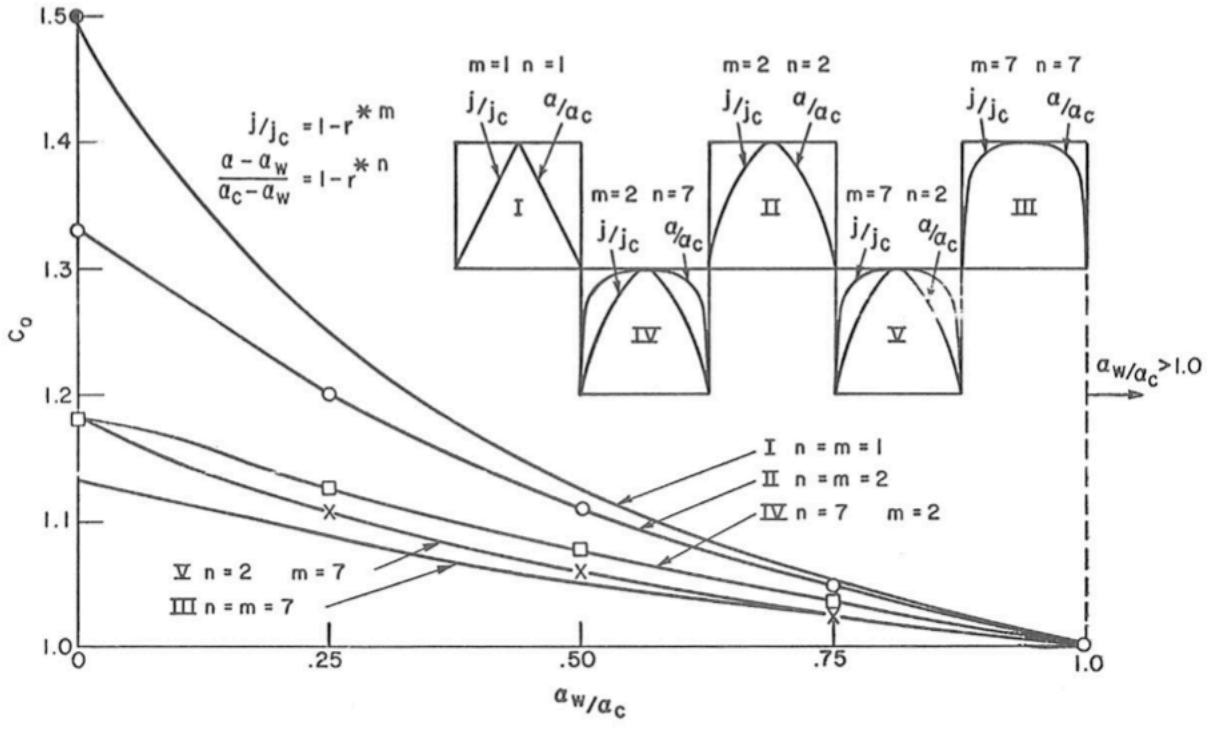

Figure 2-13 The distribution parameter vs. the ratio of void fraction next to the pipe wall and the center of the pipe for different velocity and void fraction distributions (Zuber and Findlay 1965).

There are dozens of studies after Zuber and Findlay (1965) developed correlations for the flow distribution coefficient and the drift velocity trying to capture the flow behaviors under different conditions. Table 2-1 summarizes the drift-flux correlations developed by the previous studies. The earlier studies assumed that the distribution parameter has a constant value, which is applicable only for a specific flow pattern. Hibiki and Ishii (2003) proposed three C_0 correlations for bubbly, slug, and annular flow by including the gas-liquid density ratio $\left(\frac{\rho_G}{\rho_L}\right)$ and the void fraction. Choi et al. (2012) proposed the C_0 equation based on the work of Hibiki and Ishii (2003) and Fabre and Line (1992) by considering the mixture Reynold's number in addition to the density ratio and void fraction. Based on the work of Choi et al. (2012), Bhagwat and Ghajar (2014) developed a correlation for the distribution parameter that includes various two-phase parameters such as two-phase density ratio, mixture Reynold's number, gas volumetric flow fraction, two-phase friction factor, and inclination angle.

Table 2-1 Summary of previous drift-flux models

Correlation	Distribution coeffient	Drift velocity
Zuber and Findlay (1965)	$C_0 = 1.2$	$V_d = 1.53(g\delta\Delta\rho/\rho_l^2)^{0.25}$
Greskovich and Cooper (1975)	$C_0 = 1$	$V_d = 0.671\sqrt{gD}(sin\theta)^{0.263}$
Shipley (1984)	$C_0 = 1.2$	$V_d = 0.24 + 0.35(V_{sg}/V_m)^2\sqrt{gD\alpha_g}$
Gomez et al. (2000)	$C_0 = 1.15$	$V_d = 1.53(g\delta\Delta\rho/\rho_l^2)^{0.25}(1-\alpha_g)^{0.5}$
Hibiki and Ishii (2003)	$C_0 = 1.2 - 0.2\sqrt{(\rho_g/\rho_l)}(1-\exp(-18\alpha_g))$ $C_0 = 1.2 - 0.2\sqrt{(\rho_g/\rho_l)}$ $C_0 = 1 + (1-\alpha_g)/(\alpha_g + 4\sqrt{\rho_g/\rho_l})$	$V_d = 1.41(g\delta\Delta\rho/\rho_l^2)^{0.25}(1-\alpha_g)^{1.75}$ $V_d = 0.35\sqrt{gD(\rho_l-\rho_g)/\rho_l}$ $V_d = (1-\alpha_g)\left(\alpha_g + 4\frac{\sqrt{\rho_g/\rho_l}(\sqrt{gD(\rho_l-\rho_g)/\rho_l})}{0.015\rho_g}\right)$
Shi et al. (2005)	$C_0 = \frac{A}{1+(A-1)\left(\frac{\beta-B}{1-B}\right)^2}$ $\beta = max\left(\alpha_g, F_r\frac{\alpha_g\lvert V_m\rvert}{V_{sgf}}\right)$ $V_{sgf} = K_u\sqrt{\rho_l/\rho_g}(g\delta\Delta\rho/\rho_l^2)^{0.25}$	$V_d = \frac{(1-\alpha_g C_0)C_0K(\alpha_g)(g\delta\Delta\rho/\rho_l^2)^{0.25}}{\alpha_g C_0\sqrt{\rho_g/\rho_l}+1-\alpha_g C_0}$ $K(\alpha_g) = \begin{cases} 1.53/C_0, & \alpha_g \le 0.2 \\ K_u, & \alpha_g \ge 0.4 \end{cases}$ $K_u = max\left[min\left(3.587 - \frac{19.105}{\widetilde{D}+3.333}, 3.2\right), 0\right]$ and $\widetilde{D} = \sqrt{g(\rho_l\rho_g)\sigma_g}D$
Choi et al. (2012)	$C_0 = \frac{2}{1+(Re_m/1000)^2} + \frac{1.2-0.2\sqrt{(\rho_g/\rho_l)}(1-\exp(-18\alpha_g))}{1+(1000/Re_m)^2}$	$V_d = 0.0246\times cos\theta + 1.606\times(g\delta\Delta\rho/\rho_l^2)^{0.25}sin\theta$
Bhagwat and Ghajar (2014)	$C_0 = \frac{2-(\rho_G/\rho_L)^2}{1+(Re_{TP}/1000)^2} + \frac{\left[\left(\sqrt{(1+(\rho_G/\rho_L)^2\cos\theta)/(1+\cos\theta)}\right)^{(H_L)}\right]^{2/5}+C_{0,1}}{1+(1000/Re_{TP})^2}$ $C_{0,1} = (0.2-0.2\sqrt{\rho_G/\rho_L})\times\left[\left(2.6-\frac{v_{SG}}{v_M}\right)^{0.15} - \sqrt{f_{TP}}\right]\times\left(1-\frac{m_G}{m_G+m_L}\right)^{1.5}$ $Re_{TP} = \frac{\rho_L v_M d}{\mu_L}$	$V_d = C_2C_3C_4\times(0.35sin\theta + 0.45cos\theta)\times\sqrt{gD(\rho_l-\rho_g)(1-\alpha_g)/\rho_l}$ $C_2 = \begin{cases} \left[\frac{0.434}{\lg(\mu_l/0.001)}\right]^{0.15}, & (\mu_l/0.001) > 0 \\ 1, & (\mu_l/0.001) < 0 \end{cases}$ $C_3 = \begin{cases} (La/0.025)^{0.9}, & La < 0.025 \\ 1, & La \ge 0.025 \end{cases}$ and $La = \frac{\sqrt{\sigma g/(\rho_l-\rho_g)}}{D}$ $C_4 = \begin{cases} -1, & for\ -50^\circ \le \theta \le 0^\circ\ and\ Fr_{sg} \le 0.1 \\ 1, & others \end{cases}$
Tang et al. (2019)	$C_0 = \frac{1.088}{1+0.088\times min\left\{\left[\left(\max\left(\alpha_g, \frac{\alpha_g\lvert V_m\rvert}{V_{sgf}}\right) - 0.833\right)\Big/0.167\right]^2, 1\right\}}$ $V_{sgf} = K_u\sqrt{\rho_l/\rho_g}(g\delta\Delta\rho/\rho_l^2)^{0.25}$	$V_{d,v} = \frac{(1-\alpha_g C_0)C_0K(\alpha_g)(g\delta\Delta\rho/\rho_l^2)^{0.25}}{\alpha_g C_0\sqrt{\rho_g/\rho_l}+1-\alpha_g C_0}$ $K(\alpha_g) = \begin{cases} 1.53/C_0 & ,for\ \alpha_g \le \alpha_1 \\ 1.53/C_0 + \frac{K_u - 1.53/C_0}{2}\left[1-cos\left(\pi\frac{\alpha_g-\alpha_1}{\alpha_2-\alpha_1}\right)\right] & ,for\ \alpha_1 < \alpha_g < \alpha_2 \\ K_u & ,for\ \alpha_g > \alpha_2 \end{cases}$ $V_{d,h} = \sqrt{gD}\left\{1.981 - 1.759\times\left[\frac{(N_\mu)^{0.477}}{(N_{Eo})^{0.574}}\right]\right\}[\alpha_g(1-\alpha_g)]$ $N_\mu = \frac{\mu_l}{(\rho_l-\rho_g)D^{1.5}\sqrt{g}}$ and $N_{Eo} = \frac{g((\rho_l-\rho_g)D^2}{\sigma}$ $V_d = \left(1.017\times V_{d,h}sin\theta + \left\{1 - \frac{2}{1+exp[50\times\sin(\theta+2.303V_m)]}\right\}V_{d,h}cos\theta\right)\left(1+\frac{1000}{Re_m+1000}\right)$

Tengesdal et al. (1999) proposed that the total pressure gradient could be calculated using the following equation:

$$\left(\frac{dP}{dL}\right)_{total} = \left(\frac{dP}{dL}\right)_{gravitational} + \left(\frac{dP}{dL}\right)_{frictional} \tag{2-16}$$

$$\left(\frac{dP}{dL}\right)_{total} = \rho_M\ g\ \sin\theta\ + \frac{f_M\ \rho_M\ v^2{}_M}{2d} \tag{2-17}$$

where, f_M is the Moody friction factor as a function of the mixture Reynolds number:

$$N_{Re_M} = \frac{\rho_M \, v_M \, d}{\mu_M} \tag{2-18}$$

The mixture viscosity and density can be calculated as follows:

$$\mu_M = (1-\alpha)\,\mu_L + \alpha\,\mu_g \tag{2-19}$$

$$\rho_M = (1-\alpha)\,\rho_L + \alpha\,\rho_g \tag{2-20}$$

2.2.1.3 Modified Segregated Flow Model for Churn Flow

Pagan et al. (2017) proposed a model for churn and annular flow in small and large diameter vertical and near vertical pipes. The model was proposed based on the one proposed by Jayanti and Brauner (1994) and was intended to be used for pressure from near atmospheric to 8900 psia and temperature between 25 and 450°C. The liquid entrainment in the gas core was assumed to be part of the liquid film and the gas entrainment was neglected for the purpose of simplification. Figure 2-15 shows a schematic of the force balance for the modified segregated model presented by Pagan et al. (2017). The interfacial shear stress τ_i represents the interaction between the gas and liquid phases, and the wall shear stress τ_w represents the interaction between the liquid flow and the pipe wall. The following equations express the force balance for the inner (gas) and outer (liquid) control volumes respectively.

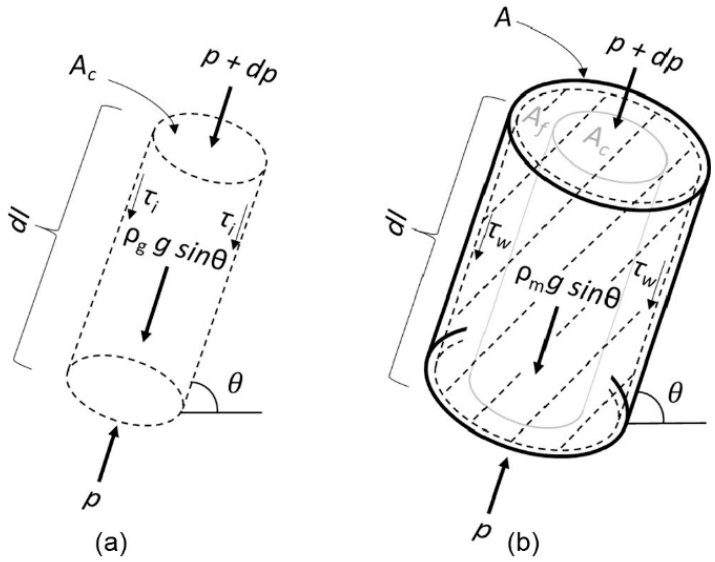

Figure 2-14 Force balance in a pipe for churn and annular flow patterns on (a) gas core and (b) cross-sectional area (Pagan et al. 2017).

$$-\frac{dP}{dL} = \frac{4\,\tau_i}{d\,\sqrt{\alpha}} + \rho_g\, g\, \sin\theta \tag{2-21}$$

$$-\frac{dP}{dL} = \frac{4\,\tau_w}{d} + [\,\rho_g \alpha + \rho_l(1-\alpha)]g\sin\theta \tag{2-22}$$

where, *dp/dL* is the pressure gradient, *d* is the pipe diameter, τ_i is the interfacial shear stress, and τ_w is the wall shear stress, given as:

$$\tau_w = \frac{1}{2}\,\rho_l\, f_l\, (\frac{v_{sl}}{1-\alpha})^2 \tag{2-23}$$

The wall friction factor for the liquid film is given by

$$f_l = \frac{16}{Re_{lf}} \qquad \text{for } Re_{lf} < 2100 \tag{2-24}$$

$$f_l = \frac{0.079}{Re_{lf}{}^{0.25}} \qquad \text{for } Re_{lf} > 2100 \tag{2-25}$$

The interfacial shear stress is given by:

$$\tau_i = \frac{1}{2} \rho_g f_i \left(\frac{v_{sg}}{\alpha}\right)^2 \quad (2\text{-}26)$$

where, the interfacial friction factor, f_i, is given by the average of the interfacial friction factor proposed by Wallis (1969), $f_{i,W}$, and Alves (2014), $f_{i,B}$:

$$f_i = \frac{f_{i,W} + f_{i,B}}{2} \quad (2\text{-}27)$$

$$f_{i,W} = 0.005 + 0.75\left(1 - \sqrt{\alpha}\right) \quad (2\text{-}28)$$

$$f_{i,B} = 0.005 + 10^{\left(-0.56 + \frac{9.07}{d^*}\right)} \left[\frac{d^* (1-\alpha)}{4}\right]^{\left(1.63 + \frac{4.74}{d^*}\right)} \quad (2\text{-}29)$$

where, d^* is the dimensionless diameter:

$$d^* = d \sqrt{\frac{\left(\rho_l - \rho_g\right) g}{\sigma}} \quad (2\text{-}30)$$

The liquid holdup is calculated from the combined momentum equation derived from Equations 2-21 and 2-22:

$$\frac{4\,\tau_i}{d\sqrt{\alpha}} + \rho_g\, g\, \sin\theta - \frac{4\,\tau_w}{d} - [\,\rho_g\,\alpha + \rho_l\,(1-\alpha)\,]\, g\, \sin\theta = 0 \quad (2\text{-}31)$$

Once the liquid holdup is determined, the pressure gradient can be calculated from either Equation 2-21 or 2-22.

2.2.2 Previous Modeling Studies on Pseudo-slug Flow

Most of the previous modeling efforts for PS flow treat it as conventional slug flow such as OLGA, TUFFP unified Zhang et al. (2003), and Xiao et al. (1990). Previous studies have shown that these models fail for pseudo-slug flow prediction.

Modeling of pseudo-slug flow has emerged in recent years after recent advanced experimental investigation on this flow pattern. There are two models available in the literature

for pseudo-slug flow. One model is based on the drift flux model, and the other is a modified unit-cell slug model.

2.2.2.1 Drift-flux Model for Pseudo-slug Flow

Soedarmo et al. (2018b) and Soedarmo (2019) developed the C_0 and v_D correlations based on Bhagwat and Ghajar (2014). The main equation of C_0 presented by Bhagwat and Ghajar (2014) is shown as follows:

$$C_0 = \frac{2-(\rho_G/\rho_l)^2}{1+(Re_{TP}/1000)^2} + \frac{\left[\left(\sqrt{(1+(\rho_G/\rho_l)^2\cos\theta)/(1+\cos\theta)}\right)^{(H_L)}\right]^{2/5} + C_{0,1}}{1+(1000/Re_{TP})^2} \quad (2\text{-}32)$$

$$C_{0,1} = \left(0.2-0.2\sqrt{\rho_G/\rho_L}\right) \times \left[\left(2.6-\frac{v_{SG}}{v_M}\right)^{0.15} - \sqrt{f_{TP}}\right] \times \left(1-\frac{m_G}{m_G+m_L}\right)^{1.5} \quad (2\text{-}33)$$

$$Re_{TP} = \frac{\rho_L v_M d}{\mu_L} \quad (2\text{-}34)$$

The main structure of the equation was first presented by Fabre and Line (1992) and used later by Choi et al. (2012). It consists of two terms and each term contains the two-phase Reynolds number, Re_{TP}, in the denominator, which accounts for the transition from low to high Reynolds number or laminar to turbulent flow. For small Re_{TP} values (Re_{TP}< 1000), the first term becomes dominant and the second term is nominal; while it is the opposite for large Re_{TP}, i.e., the second term becomes more dominant when Re_{TP} increases from 1000. It has been observed by several studies that C_0 presents two regions depending on the Reynolds number. Fabre (1994) showed that C_0 approaches to 2 when the flow is laminar, and it is close to 1.2 when it is turbulent flow, as illustrated in Figure 2-16.

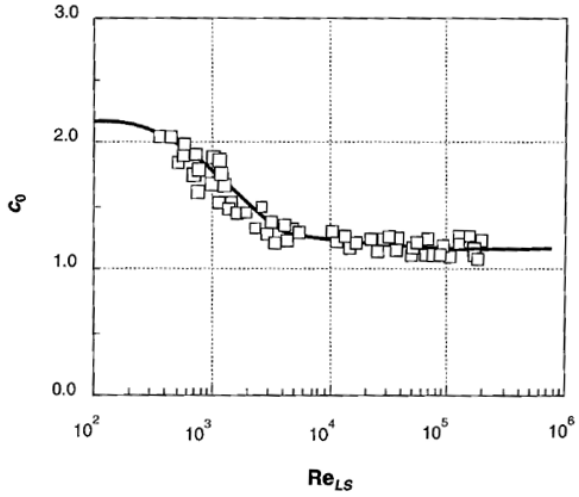

Figure 2-15 Experimental Results for C_0 (after Fabre 1994).

Figures 2-17 and 2-18 show the C_0 value as a function of Re_{TP} estimated by Bhagwat and Ghajar (2014) for different $C_{0,1}$ and $\frac{\rho_G}{\rho_L}$ values respectively. The flat line for the lower values of Re_{TP} represents the numerator of the first term in Equation 2-32, and the flat line for the higher Re_{TP} values is the numerator of the second term in Equation 2-32. Bhagwat and Ghajar's (2014) correlation for the C_0 accounts for phase density ratio, gas volumetric flow fraction, two phase flow quality, pipe orientation, and two-phase friction factor.

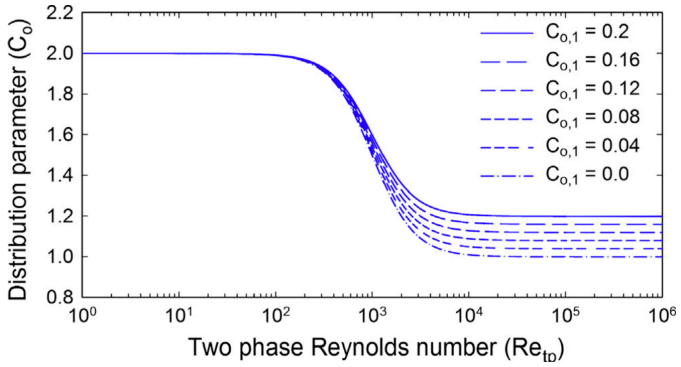

Figure 2-16 Distribution parameter C_0 as a function of two-phase Reynold's number Re_{TP} for different $C_{0,1}$ values (Bhagwat and Ghajar 2014).

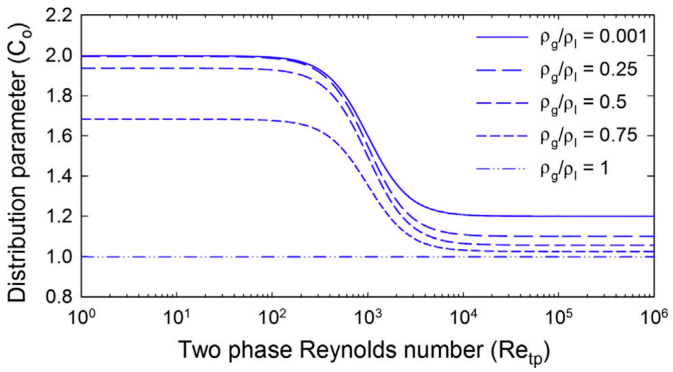

Figure 2-17 Distribution parameter C_0 as a function of two-phase Reynold's number Re_{TP} for different density ratios (Bhagwat and Ghajar 2014).

The effect of the pipe inclination and liquid holdup presented in the second term of the equation, $\left(\sqrt{(1+(\rho_G/\rho_l)^2\cos\theta)/(1+\cos\theta)}\right)^{(H_L)}$, is formulated in a way that puts more weight on the pipe orientation in the case of higher values of the liquid holdup (bubbly or slug flows) and approaches to unity in the case of lower values of the liquid holdup (annular flow). The effect of the gas to liquid density ratio $\frac{\rho_G}{\rho_L}$ on C_0 by Bhagwat and Ghajar (2014) is illustrated in Figure 2-18. It shows that in the case when the density ratio equals one $\left(\frac{\rho_G}{\rho_L}=1\right)$, the C_0 will approach to unity since the mixture will practically be a single phase. The $C_{0,1}$ in Equation 2-32 considers the two-phase flow quality $\frac{m_G}{m_G+m_L}$, gas volumetric flow fraction $\frac{v_{SG}}{v_M}$, and two-phase friction factor f_{TP}, such that C_0 will be a decreasing function of the void fraction and sensitive to lower values of void fraction.

The drift velocity correlation presented by Bhagwat and Ghajar (2014) is modeled as a function of pipe diameter, pipe inclination, fluid properties, and the void fraction, as given by:

$$v_D = (0.35\sin\theta + 0.45\cos\theta)\sqrt{\frac{gd(\rho_L-\rho_G)}{\rho_L}}(H_L)^{0.5}C_2C_3 \tag{2-35}$$

$$C_2 = \begin{cases} (0.434/\log_{10}(1000\mu_L))^{0.15} & ;\text{for } \left(1000\mu_L\right) > 10 \\ 1 & ;\text{otherwise} \end{cases} \tag{2-36}$$

$$C_3 = \begin{cases} \left(\frac{1}{0.025}\left(\sqrt{\frac{\sigma}{g\left(\rho_L - \rho_G\right)d^2}}\right)\right)^{0.9} & ;\text{for } \left(\sqrt{\frac{\sigma}{g\left(\rho_L - \rho_G\right)d^2}}\right) < 0.025 \\ 1 & ;\text{otherwise} \end{cases} \tag{2-37}$$

The equation combines the drift velocities at vertical and the horizontal pipes. The vertical drift velocity is based on Davies and Taylor (1950) and Dumitrescu (1943), given as $v_{d,v} = 0.35\sqrt{gd}$, and the horizontal drift velocity equation is based on (Benjamin 1968), given as $v_{d,h} = 0.54\sqrt{gd}$. Bendiksen (1984) presented a correlation for the drift velocity in upward inclined pipes by combining the vertical and the horizontal drift velocity equations, $v_d = 0.35\sqrt{gd}\sin\theta + 0.54\sqrt{gd}\cos\theta$. Bhagwat and Ghajar (2014) modified the proportionality constant for horizontal drift velocity to 0.45 instead of 0.54 based on experimental data from Gokcal et al. (2009).

Soedarmo et al. (2018b) proposed a new correlation by adjusting the proportionality constants in Bhagwat and Ghajar's (2014) model specifically for pseudo-slug flow in upward inclined pipes based on data from Fan (2017), Alsaadi et al. (2015), and Langsholt and Holm (2007). The correlations are given below:

$$C_0 = \frac{2 - (\rho_G/\rho_l)^2}{1 + (Re_{TP}/1000)^2} + \frac{\left[\left(\sqrt{(1 + (\rho_G/\rho_l)^2\cos\theta)/(1 + \cos\theta)}\right)^{(H_L)}\right]^{-1.9} + C_{0,1}}{1 + (1000/Re_{TP})^2} \tag{2-38}$$

$$Re_{TP} = \frac{\rho_L v_M d}{\mu_L} \tag{2-39}$$

$$C_{0,1} = \left(0.2 - 0.2\sqrt{\rho_G/\rho_L}\right) \times \left[\left(1.0 - \frac{v_{SG}}{v_M}\right)^{0.28} - \sqrt{f_{TP}}\right] \times \left(1 - \frac{m_G}{m_G + m_L}\right)^{1.15} \tag{2-40}$$

$$v_D = \begin{cases} (0.35\sin\theta + 0.54\cos\theta)\sqrt{\dfrac{gd(\rho_L - \rho_G)}{\rho_L}}\, C_2 C_3 (H_L)^{(\rho_G/\rho_l)^{C_5}} & ; \text{for } (C_5) < 2 \\ (0.35\sin\theta + 0.54\cos\theta)\sqrt{\dfrac{gd(\rho_L - \rho_G)}{\rho_L}}\, C_2 C_3 & ; \text{otherwise} \end{cases} \quad (2\text{-}41)$$

$$C_2 = \begin{cases} (0.434/\log_{10}(1000\mu_L))^{0.15} & ; \text{for } (1000\mu_L) > 10 \\ 1 & ; \text{otherwise} \end{cases} \quad (2\text{-}42)$$

$$C_3 = \begin{cases} \left(\dfrac{1}{0.03}\left(\sqrt{\dfrac{\sigma}{g(\rho_L - \rho_G)d^2}}\right)\right) & ; \text{for } \left(\sqrt{\dfrac{\sigma}{g(\rho_L - \rho_G)d^2}}\right) < 0.03 \\ 1 & ; \text{otherwise} \end{cases} \quad (2\text{-}43)$$

$$C_5 = 5.2765 \times 10^8 \left(Re_{TP}\frac{\rho_G}{\rho_L}\right)^{-2.434} \quad (2\text{-}44)$$

2.2.2.2 Modified Unit-cell Model

Unit-cell model is a conventional approach to model slug flow. Soedarmo (2019) presented modifications to the conventional slug unit-cell model for pseudo-slug flow by assuming a continuous gas passage, slippage, and interfacial momentum exchange in the pseudo-slug body or waves. It is worth mentioning that the gas slippage in the slug body in the slug unit cell model is commonly assumed to be zero and both gas and liquid move at the mixture velocity. It is also assumed that the liquid and gas entrainment can be neglected in the liquid film and slug regions for simplicity. Figure 2-19 illustrates the momentum equations of the modified unit-cell model for pseudo-slug flow proposed by Soedarmo (2019).

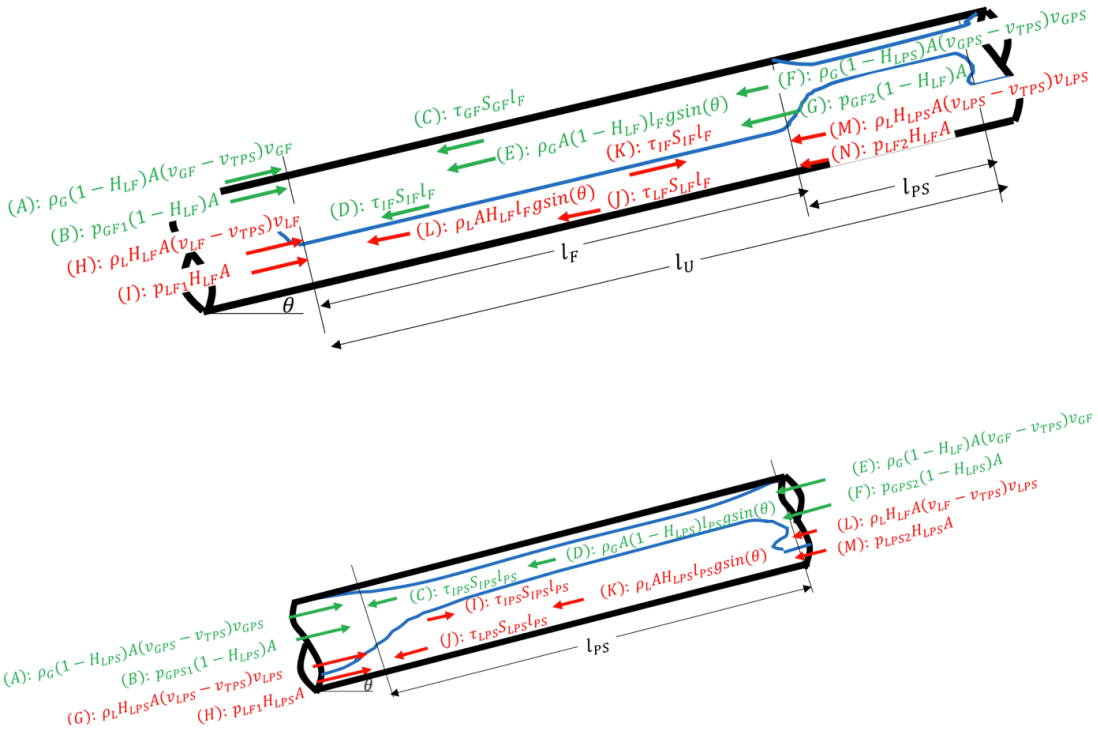

Figure 2-18 Illustration of combined momentum equation for modified unit cell model for pseudo-slug flow (Soedarmo et al. 2018a).

The general concept of the modified unit-cell model is to divide the pseudo-slug flow into two regions, the film and the pseudo-slug body, considering gas slippage in the film region as well as in the pseudo-slug body region. The continuity equations for the film region are given in Equations 2-45 to 2-48. Two combined momentum equations for the film and pseudo-slug body are described in Equations 2-49 and 2-50 respectively.

$$l_U v_{SL} = l_{PS} v_{LPS} H_{LPS} + l_F v_{LF} H_{LF} \tag{2-45}$$

$$l_U v_{SG} = l_{PS} v_{GPS}(1 - H_{LPS}) + l_F v_{GF}(1 - H_{LF}) \tag{2-46}$$

$$H_{LPS}(v_{TPS} - v_{LPS}) = H_{LF}(v_{TPS} - v_{LF}) \tag{2-47}$$

$$(1 - H_{LPS})(v_{TPS} - v_{GPS}) = (1 - H_{LF})(v_{TPS} - v_{GF}) \tag{2-48}$$

$$\frac{\rho_L(v_{LF}-v_{TPS})(v_{LF}-v_{LPS})-\rho_G(v_{GF}-v_{TPS})(v_{GF}-v_{GPS})}{l_F}$$
$$+\tau_{IF}S_{IF}\left(\frac{1}{A_{LF}}+\frac{1}{A_{GF}}\right)-\frac{\tau_{LF}S_{LF}}{A_{LF}}+\frac{\tau_{GF}S_{GF}}{A_{LF}}-(\rho_L-\rho_G)gsin\,\theta\ =0 \quad (2\text{-}49)$$

$$\frac{\rho_L(v_{LPS}-v_{TPS})(v_{LPS}-v_{LF})-\rho_G(v_{GPS}-v_{TPS})(v_{GPS}-v_{GF})}{l_{PS}}$$
$$+\tau_{IPS}S_{IPS}\left(\frac{1}{A_{LPS}}+\frac{1}{A_{GPS}}\right)-\frac{\tau_{LPS}S_{LPS}}{A_{LPS}}-(\rho_L-\rho_G)g\ sin\,\theta\ =0 \quad (2\text{-}50)$$

These two combined momentum equations are solved primarily to obtain the film length or liquid holdup in the film region. The model requires three typical closure relationships for the translational velocity, slug body holdup, and slug body length. These closure relationships were developed based on previously available pseudo-slug flow data. They are presented in Soedarmo et al. (2018a) and updated in Soedarmo (2019) by including some high-pressure pseudo-slug flow data from Soedarmo (2019) and Rodrigues (2018). It is worth mentioning that their modified unit-cell model requires the liquid holdup prediction from the aforementioned drift-flux model proposed by Soedarmo et al. (2018b) for the sake of simplicity. One of the advantages of the unit-cell model is that it also predicts flowing parameters, such as frequency, slug length, etc., in addition to pressure gradient and liquid holdup, which could be useful for production design and operation.

CHAPTER 3
MODELING PSEUDO-SLUG AND CHURN FLOWS

This chapter first discusses the datasets used for the model development, followed by the explanation of the new model, and comparison with other current existing models from literature.

3.1 Experimental Datasets of Pseudo-slug and Churn Flows

Table 3-1 summarizes the previous experimental studies for the pseudo-slug and churn flows. The experimental data sets cover different pipe diameters, pressures (or gas densities), inclination angles, and liquid viscosities. These data sets were used in the model development for the current study. In summary, most of these studies used air and water as the testing fluids in their experiments, while a few used oil or mixture of water and CMC (Carboxymethylcellulose) with different viscosities. The pipe diameter ranges from 0.032 m to 0.189 m, and the pipe inclination variates from slightly inclined to vertical (0.5° to 90°). Most of the pseudo-slug flow experiments in the table have the measurements of both liquid holdup and pressure gradient. For the churn flow studies, three of them (van der Meulen, 2012; Zhu 2020; and Skopich, 2012) have measured both liquid holdup and pressure gradient, while Parsi et al. (2015ab) and Abdulkadir et al. (2019) only reported the liquid holdup, and Owen (1986) only presented data on the pressure gradient measurement. There is a total of 1431 data points from the previous experimental studies combined. Figure 3-1 shows the data distribution for each nine parameters, including inclination angle, pipe diameter, superficial liquid velocity, superficial gas velocity, liquid and gas densities, liquid and gas viscosities, and surface tension.

Table 3-1 Experimental Conditions of Previous Experiments on PS and CH Flows

Authors	**Testing Fluids**	***d*** **(m)**	***θ*** **(°)**	***p*** **(psia)**	μ_L **(cp)**	v_{SL} **(m/s)**	v_{Sg} **(m/s)**	**FP**	**Measurement**
(Fan et al. 2019)	Air, Water	0.0762	2 - 20	14.7	1	0.001 - 0.01	2 - 32	PS, SEG	dp/dL, H_L
(Alsaadi et al. 2015)	Air, Water	0.0762	2 - 30	14.7	1	0.01 - 0.1	2 - 32	PS, SEG	dp/dL, H_L
(Guner 2012)	Air, Water	0.0762	45 - 90	14.7	1	0.01 - 0.1	2 - 32	PS/CH, SEG	dp/dL, H_L
(Rodrigues et al. 2019)	N_2, Oil	0.155	2	200-400	1.3	0.01 - 0.05	1.4 - 16.5	SL, PS, SEG	dp/dL, H_L
(Alsaadi 2019)	Air, Water	0.155	2	14.7	1	0.005 - 0.05	3 - 30	SL, PS, SEG	dp/dL, H_L
(Soedarmo 2019) (LPHV)	Air, ND50	0.0508	5, 45, 85	14.7	213	0.05 - 2	1 - 16	SL, PS/CH, SEG	dp/dL, H_L
(Soedarmo 2019) (HPLV)	N_2, Oil	0.155	2	200-400	1.3	0.01 - 0.05	1.4 - 16.5	SL, PS, SEG	dp/dL, H_L
(Langsholt and Holm 2007)	SF6, Oil/Water	0.1524	0.5 - 5	51 - 103	1, 1.8	0.001	1 - 3	PS, SEG	H_L
(Zhu 2019)	Air, Water	0.1016	2 - 90	80	1	0.05	0.1 - 4	SL, PS/CH	dp/dL, H_L
(Kjølaas et al 2018)	Nitrogen, Nexbase 3080	0.189	0.5	652	94.3	1,1.5,2	0.003 - 4	PS	dp/dL, H_L
(Parsi et al. 2015a)	Air, Water with CMC	0.0762	90	14.7	1,10,40	0.46 - 0.76	10 - 27	SL, CH, AN	H_L
(Parsi et al. 2015b)	Air, water	0.0762	90	14.7	1	0.3 - 0.76	10 - 38	CH, AN	H_L
(Abdulkadir et al. 2019)	Air, water	0.127	90	14.7	1	0.02 - 0.33	3.5 - 16.1	CH, AN	H_L
(Skopich 2012)	Air, water	0.0508, 0.1016	90	14.7	1	0.01 - 0.05	10 - 30	CH, AN	dp/dL, H_L
(Van der Meulen 2012)	Air, water	0.13	90	14.7	1	0.004-0.7	3 - 20	CH, AN	dp/dL, H_L
(Owen 1986)	Air, water	0.032	90	35	1	0.005 - 0.4	2 - 22	CH	dp/dL

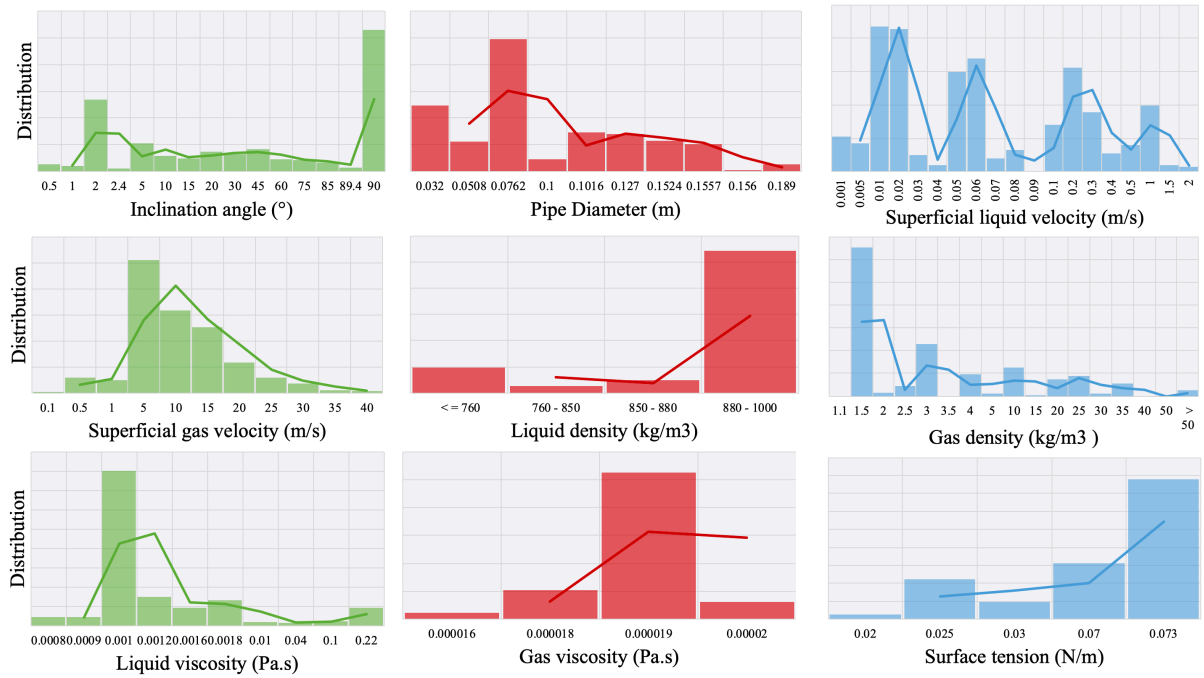

Figure 3-1 Data distribution for different parameters from the experimental dataset.

3.2 New Model Development

This section discusses the development of the drift velocity, flow distribution coefficient, and the model for the pressure gradient prediction, respectively. In the new model, the liquid holdup is predicted using drift-flux model with new correlations of drift velocity and flow distribution coefficient. The main function of the drift-flux model is given in Equation 3-1, where α is the void fraction, H_L is the liquid holdup, v_{SG} is the superficial gas velocity, v_{SL} is the superficial liquid velocity, v_G is the actual gas velocity, v_M is the mixture velocity, C_0 is the flow distribution coefficient, and v_D is the drift velocity.

$$\alpha = 1 - H_L = \frac{v_{SG}}{v_G} = \frac{v_{SG}}{C_0 v_M + v_D} = \frac{v_{SG}}{C_0(v_{SG}+v_{SL})+v_D} \tag{3-1}$$

Considering the non-uniform distribution of the gas and liquid phases at the pipe cross-section area in an inclined pipe, we propose to use the two-fluid model for pressure gradient prediction using liquid holdup predicted from the aforementioned drift flux model.

3.2.1 Modeling Drift Velocity

The gas phase can flow faster upward than the liquid phase due to the buoyancy. Drift velocity reflects the velocity of the gas phase in a stagnant liquid column as a result of the density difference. Previous experimental data showed that the factors that mainly impact the drift velocity are the liquid viscosity, pipe diameter, density difference, and inclination angle. The drift velocity decreases with increasing liquid viscosity due to the elevated friction at the gas-liquid interface (Gokcal et al. 2009). And the drift velocity increases with increasing pipe diameter due to the reduced friction surrounding the bubbles. However, previous study claimed that the drift velocity was no longer a function of the pipe diameter in extremely large diameter pipes since the bubble may be far from the pipe wall (Kataoka and Ishii 1987).

We improved the correlation based on the experimental data from Gokcal et al. (2009) by mainly incorporating the liquid viscosity effects. The formula is given as follows:

$$v_D = v_{D@1cp} + C\left[exp\left(-\frac{\mu_L - 0.001}{0.3}\right) - 1\right] \tag{3-2}$$

$$v_{D@1cp} = (0.45\cos\theta + 0.35\sin\theta)\sqrt{\frac{gd(\rho_L - \rho_g)}{\rho_L}} \tag{3-3}$$

$$C = \begin{cases} 0.16 & \text{if } \theta \le \frac{2}{9}\pi \\ -4.3 \times 10^{-5}\left(\theta - \frac{2}{9}\pi\right)^2 + 0.16 & \text{if } \theta > \frac{2}{9}\pi \end{cases} \tag{3-4}$$

The drift velocity Equation 3-2 consists of two terms. The first term, $v_{D@1cp}$, is the drift velocity when the liquid viscosity equals 1cp. It is taken from the correlation originally proposed by Bendiksen (1984) and employed by many studies afterward (Bhagwat and Ghajar 2014). The second term is to account for the viscosity effect on the drift velocity, which also depends on the inclination angle. The data shows that the viscosity effect on the drift velocity remains almost constant for inclination angle less than 40°, but gradually reduces as the inclination angle

increases from 40° to 90°. We considered this phenomenon by including a coefficient C as a function of inclination angle in the second term of Equation 3-2. The comparison between model prediction and experimental measurement from Gokcal et al. (2009) is shown in Figure 3-2, in which the points are the experimental measurement for different liquid viscosities and the lines are the corresponding model predictions.

In addition to the liquid viscosity and inclination angle, we propose to set a critical pipe diameter boundary, beyond which the drift velocity becomes independent of pipe diameter. In this study, we used 0.1m as the critical pipe diameter based on the statement from Kataoki and Ishi (1987) that the drift velocity value is increasing with increasing pipe diameter up to about 0.1 m and does not change much for diameter values of higher than 0.1m based on the observation from previous experimental studies.

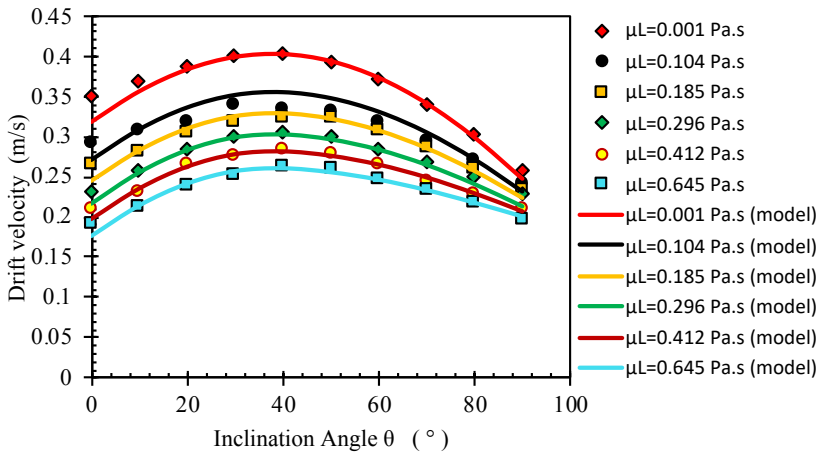

Figure 3-2 Experimental drift velocity for different liquid viscosity and inclination angles (data from Gokcal et al. 2009).

3.2.2 Modeling Flow Distribution Coefficient

The flow distribution coefficient reflects the distribution of the void fraction (or liquid holdup) and mixture velocity at the pipe cross section. Based on the previous experimental studies, the flow distribution coefficient should depend on the Reynolds number, gas void fraction, flow rates, inclination angle and pipe diameter, and fluid properties.

In this study, the distribution parameter equation is constructed considering the effects of different parameters, using the back calculated C_0 with the new v_D correlation. The equation consists of two terms as given in Equations 3-5. The first term represents the C_0 for low Reynolds numbers when the flow approaches to laminar flow (i.e., Re_{TP} < 2000), and the second term represents the C_0 for high Reynolds numbers when the flow is close to turbulent flow (i.e., when Re_{TP} > 2000). For flowing conditions with low Reynolds numbers, the second term is nominal and the first term is dominated; while it is opposite for flowing conditions with high Reynolds numbers.

$$C_0 = \frac{1.58-\left(\rho_g/\rho_L\right)^2}{1+\left(\frac{Re_{TP}}{2000}\right)^4} + \frac{C_{0HR}}{1+\left(\frac{2000}{Re_{TP}}\right)^4} \tag{3-5}$$

$$\ln C_{0HR} = AH_L + BH_L^2 + C + D(H_{Lcr} - H_L)^{1.5} \tag{3-6}$$

C_{0HR} is the flow distribution coefficient for flowing conditions with high Reynolds numbers. It consists of four terms, and the each considered different phenomenon as described below.

The $\ln C_{0HR}$ has established a linear relationship with H_L for high liquid flow rate and low pressure conditions. This phenomenon is modeled by the first and third terms in Equation 3-6. The coefficient A determines the slope of the linear relationship between $\ln C_{0HR}$ and H_L, and C determines the intercept. The coefficient A is a function of pipe diameter, inclination angle, and

the liquid viscosity. Experimental data shows that it decreases with pipe diameter based on the data from Parsi et al. (2015ab) and van der Meulen (2012) for vertical pipes as shown in Figure 3-3. However, the experimental data in inclined pipes shows that the pipe diameter effect on the slope becomes less noticeable when the pipe deviates from vertical to horizontal (Fan, 2018; Al-Saadi, 2013; Guner 2013; Al-Saadi 2019). It also variates slightly with increasing liquid viscosity based on data from Parsi et al. (2015a) (Figure 3-4).

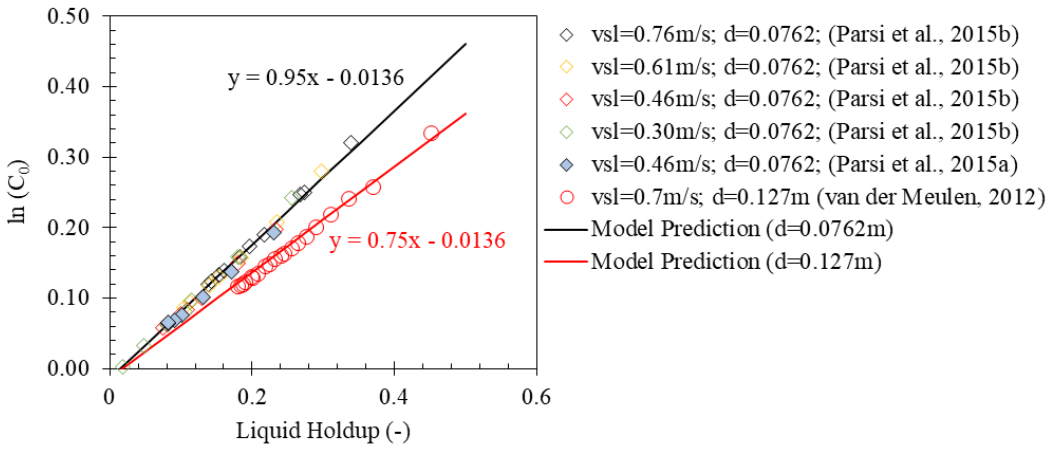

Figure 3-3 The relationship between ln C_0 and H_L (data from Parsi et al. 2015b and van der Meulen 2012).

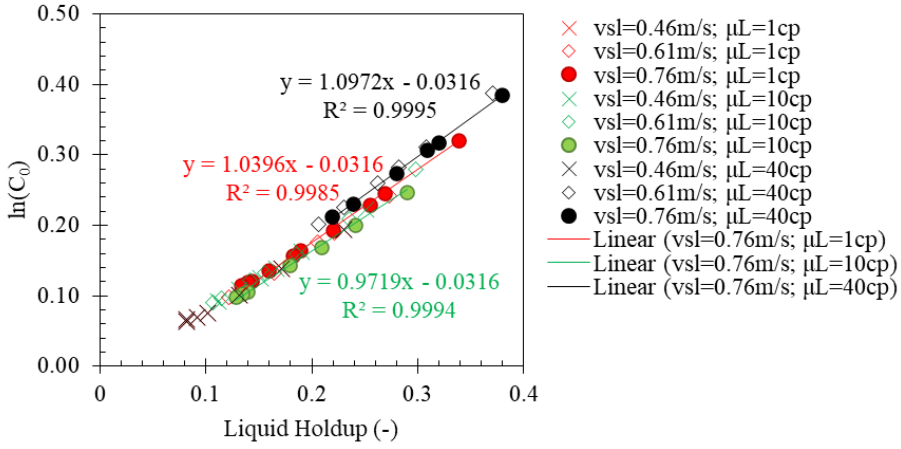

Figure 3-4 The relationship between ln C_0 and H_L (data from Parsi et al. 2015a).

Based on these observations, we propose the following equation for the coefficient A. A_{90} is the A when the inclination angle from horizontal, θ, is 90°, which decreases gradually with increasing pipe diameter or decreasing liquid viscosity. We set the upper and lower pipe diameter boundaries at 0.1016m and 0.0508m, between which majority of the experimental data locates. The purpose is to minimize the uncertainties if one uses the model outside of the experimental condition used for the model development. The A_{min} is the minimum value that A can be reached at, which is a function of inclination angle.

$$A = max(A_{90}, A_{min}) \tag{3-7}$$

$$A_{90} = \begin{cases} 1.07(2.1\mu_L + 0.996), & d \leq 0.0508 \\ (-62d^2 + 3.1496d + 1.07)(2.1\mu_L + 0.996), & 0.0508 < d < 0.1016 \\ 0.75(2.1\mu_L + 0.996), & d \geq 0.1016 \end{cases} \tag{3-8}$$

$$A_{min} = \begin{cases} 0.93, & \theta \leq \frac{\pi}{4} \\ -0.22918\left(\theta - \frac{\pi}{4}\right) + 0.93, & \theta > \frac{\pi}{4} \end{cases} \tag{3-9}$$

The coefficient C in Equation 3-6 determines the intercept of the straight line, which has been observed to be decreasing with increasing gas density, based on gas density data of higher than 10 kg/m^3 from Rodrigues (2018) and Soedarmo-HP (2019) (Figures 3-5, 3-6, and 3-7). Based on this observation, we propose the following equation for the coefficient C.

$$C = f(x) = \begin{cases} -0.0136, & \rho_g < 10 \\ 8 \times 10^{-5}\left(\frac{\rho_g}{1.225}\right)^2 - 0.0083\left(\frac{\rho_g}{1.225}\right) - 0.0049, & \rho_g \geq 10 \end{cases} \tag{3-10}$$

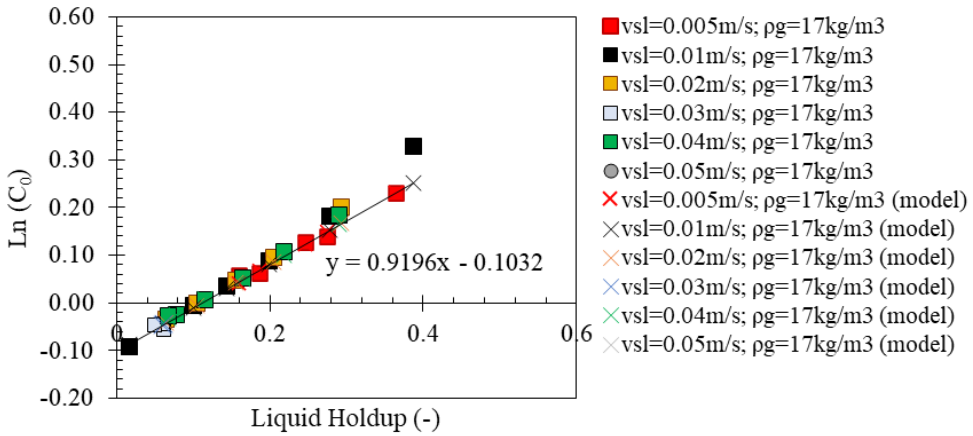

Figure 3-5 The relationship between ln C_0 and H_L at gas density of 17 kg/m^3 (data from Rodrigues 2018 and Soedarmo 2019).

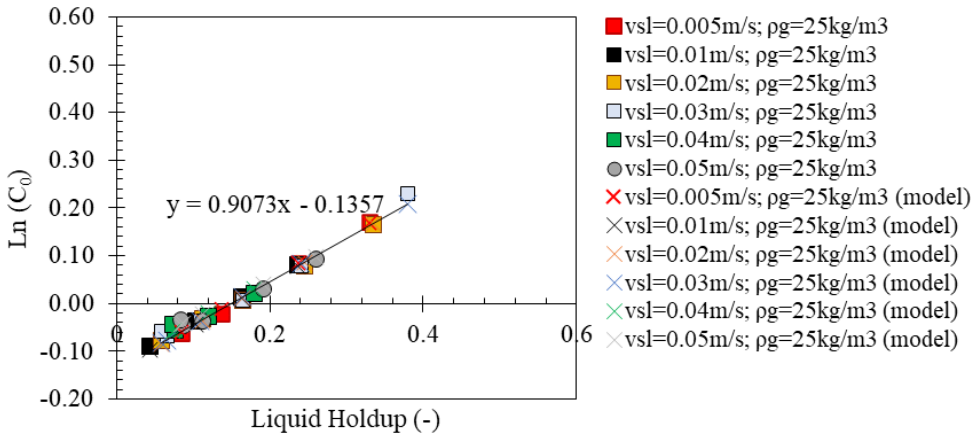

Figure 3-6 The relationship between ln C_0 and H_L at gas density of 25 kg/m^3 (data from Rodrigues 2018 and Soedarmo 2019).

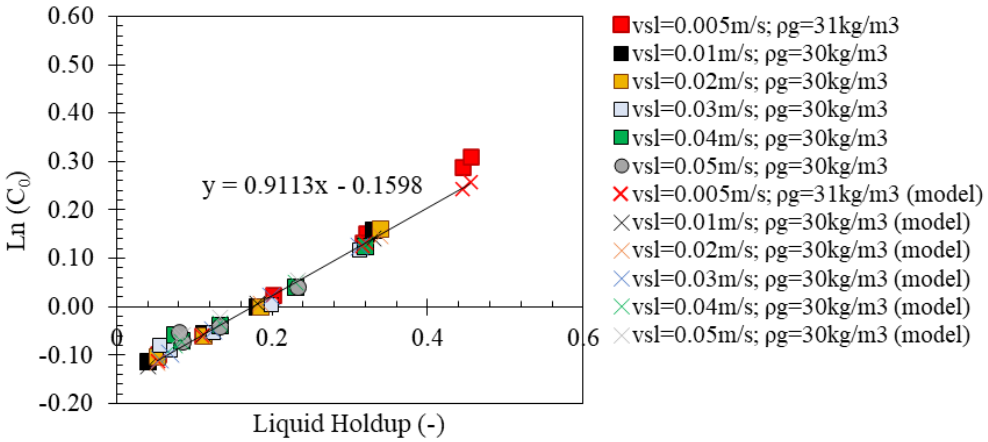

Figure 3-7 The relationship between ln C_0 and H_L at gas density of 31 kg/m^3 (data from Rodrigues 2018 and Soedarmo 2019).

The second term in Equation 3-6, BH_L^2, determines the deviation from the straight line as a function of liquid flow rate. Please note that the slope of the straight line is determined by A, which is a function of pipe diameter, liquid viscosity, and inclination angle, as discussed earlier. It has been observed that the C_0 (or liquid holdup) decreases with decreasing v_{SL} until reaching a minimum, i.e., B should variate from 0 to B_{min}, the minimum that B can be reached at (Figure 3-8). When B equals to 0, the relationship between ln C_0 and H_L is linear (when D in Equation 3-6 also equals 0, which will be discussed later). B_{min} reflects the minimum liquid holdup for a given condition regardless of the liquid flow rate. We anticipate this minimum to be close to the net-zero-liquid-flow (NZLF) condition (Amaravadi et al. 1998).

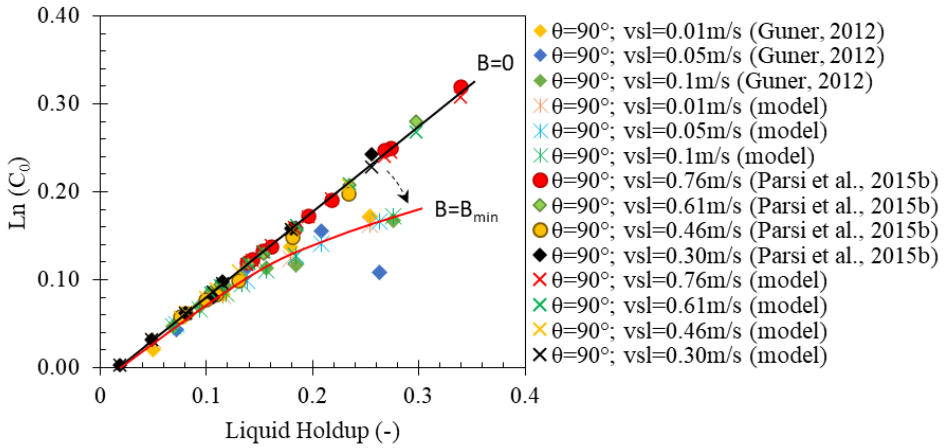

Figure 3-8 The relationship between ln C_0 and H_L for the different liquid flow rates (data from Guner 2012 and Parsi et al. 2015b at θ = 90°).

B_{min} is a function of pipe diameter, inclination angle, and gas density. It has been observed that, B_{min} decreases with increasing pipe diameter at high inclination angles but remains almost constant when the inclination angle is small. Figures 3-9 and 3-10 illustrate the effect of liquid flow rate effect on ln C_0 for inclination angles of 90° and 2°, respectively. It tells that the liquid flow rate effect on C_0 (or H_L) is more severe in larger diameter pipes at high inclination angles, while it is less obvious for slightly inclined pipes. On the other side, B_{min} increases with increasing gas density, which can be inferred from data of Rodrigues (2018) and Soedarmo (2019) shown in Figures 3-5 to 3-7. They show a nominal v_{SL} effect on C_0 even for very low liquid flow rate. It also tells that the effect of v_{SL} on C_0 (or H_L) is less obvious at high gas density conditions. Besides, we observed that, for small diameter pipes, B starts to decrease from 0 when the liquid velocity is less than 0.3 m/s approximately and becomes constant when v_{SL} is less than around 0.1m/s based on data from Guner (2012), Parsi et al. (2015b), Fan (2017), and Al-Saadi (2013); while for large diameter pipes, B starts to decrease from 0 at a higher v_{SL} (we assumed 0.7 m/s based on data from Abdulkadir et al. (2019) and van der Meulen (2012)).

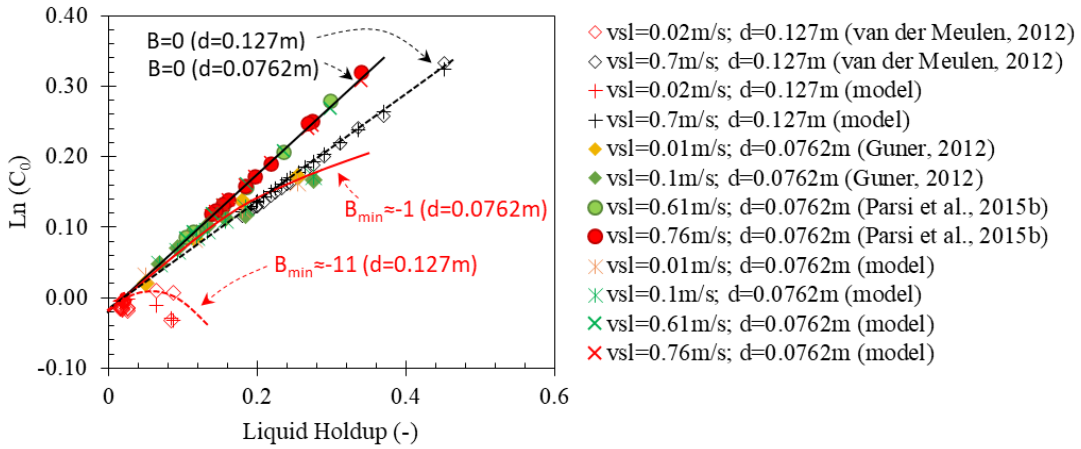

Figure 3-9 The relationship between ln C_0 and H_L for the different pipe diameters and liquid flow rates in vertical pipes (data from van der Meulen 2012, Guner 2012, and Parsi et al. 2015b).

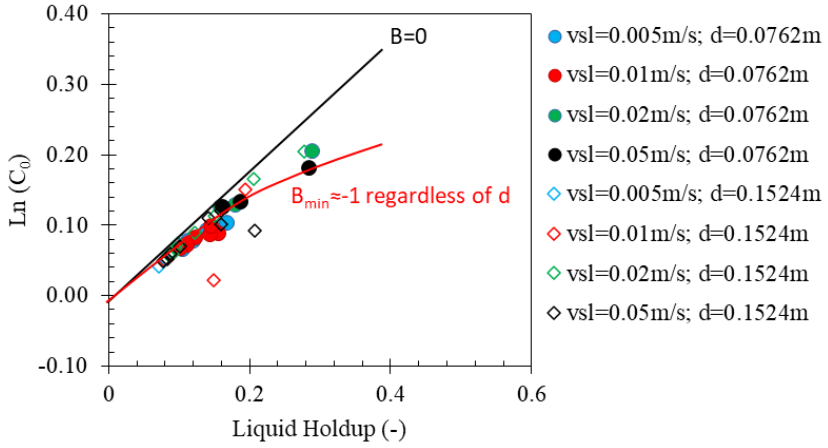

Figure 3-10 The relationship between ln C_0 and H_L for the different pipe diameters and liquid flow rates in pipes with 2° inclination angle (data from Al-Saadi 2013 and Al-Saadi 2019).

With these observations, we proposed the following equation for B. The term in the first parenthesis of B_{min} accounts for the gas density effect on B_{min}, and the second term accounts for the diameter and inclination angle effects on B_{min}.

$$B = \begin{cases} B_{min}, & v_{SL} \le 0.1m/s \\ -\frac{B_{min}(v_{SL}-0.1)}{v_{SLmax}-0.1} + B_{min}, & 0.1m/s < v_{SL} < v_{SLmax} \\ 0, & v_{SL} \ge v_{SLmax} \end{cases} \quad (3\text{-}11)$$

$$B_{min} = -\left(\frac{1}{1+\left(\rho_g/_{10}\right)^{20}}\right)\left(\frac{d}{0.0762}\right)^{n} \tag{3-12}$$

$$n = \begin{cases} 0, \ d < 0.12 \ or \ \theta < \frac{\pi}{4} \\ 4.7\left(\left(\theta - \frac{\pi}{4}\right)/\frac{\pi}{4}\right)^{10}, \ \text{else} \end{cases} \tag{3-13}$$

$$v_{SLmax} = \begin{cases} 0.3, \ d \leq 0.0762 \\ \frac{0.4(d-0.0762)}{0.0508} + 0.3, \ 0.0762 < d < 0.127 \\ 0.7, \ d \geq 0.127 \end{cases} \tag{3-14}$$

The last term in Equation 3-6, $D(H_{Lcr} - H_L)^{1.5}$, determines the upward deviation from the straight line at high liquid and gas flow rates (or low liquid holdup) conditions. This phenomenon is only observed at high gas density conditions, which is related to the transition region between segregated to intermittent flow (Rodrigues, 2018 and Soedarmo, 2019). It has been observed that $\ln C_0$ starts to deviate upward from the straight line when v_{SL} increases from 0.03 m/s, and then remains constant at a v_{SL} of 0.1 m/s, approximately. Besides, the higher the gas density, the larger H_L when $\ln C_0$ starts to deviate, which is referred to as the critical liquid holdup, H_{Lcr}, in this study. Figures 3-11 to 3-13 illustrate this phenomenon using data from Rodrigues (2018) and Soedarmo (2019). The critical liquid holdup increases from 0.2 to 0.27 when the gas density increases from 17 to 30 kg/m^3. Please also note that this deviation was not noticed for other datasets with low gas density less than 10 kg/m^3. In another word, the critical liquid holdup approaches to 0 at low gas density conditions. The coefficient D determines the magnitude apart from the straight line, and variates from 0 to 1 depending on the liquid flow rate. Based on this observation, we propose the following equation for H_{Lcr} and D. The lines in Figures 3-11 to 3-13 are from the new model prediction with different values of D. All the other

coefficients (A, B, and C in Equation 3-6) are determined from the new correlations introduced above.

$$H_{Lcr} = f(x) = \begin{cases} 0, & \rho_g \leq 10 \\ 0.0063\frac{\rho_g}{1.225} + 0.1217, & 10 < \rho_g < 40 \\ 0.3, & \rho_g \geq 40 \end{cases} \quad (3\text{-}15)$$

When $H_L > H_{Lcr}$, D = 0, otherwise:

$$D = \begin{cases} 0, & v_{SL} \leq 0.03\ m/s \\ \frac{v_{SL}-0.03}{0.97}, & 0.03\ m/s < v_{SL} < 0.1\ m/s \\ 1, & v_{SL} \geq 0.1\ m/s \end{cases} \quad (3\text{-}16)$$

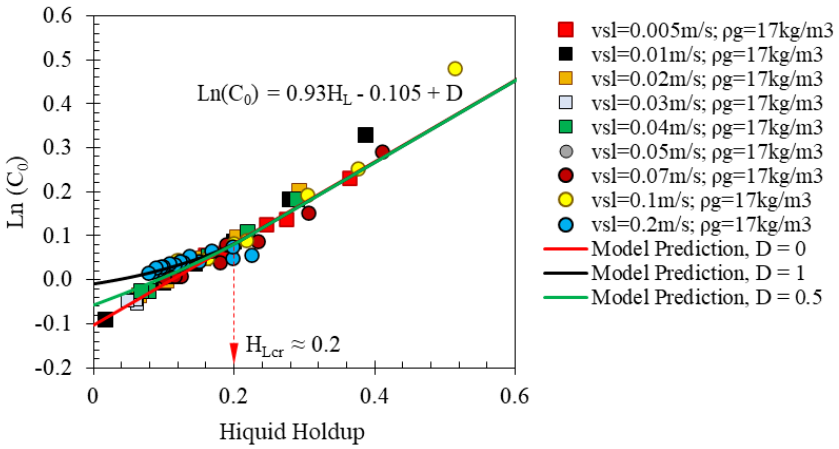

Figure 3-11 The relationship between ln C_0 and H_L for the different liquid flow rates in a 2° upward inclined pipe when gas density is 17 kg/m^3 (data from Soedarmo 2019 and Rodrigues 2018).

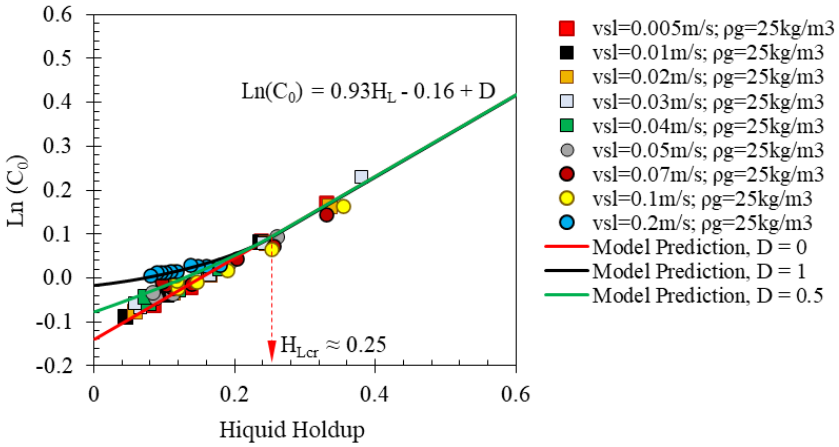

Figure 3-12 The relationship between ln C_0 and H_L for the different liquid flow rates in a 2° upward inclined pipe when gas density is 25 kg/m^3 (data from Soedarmo 2019 and Rodrigues 2018).

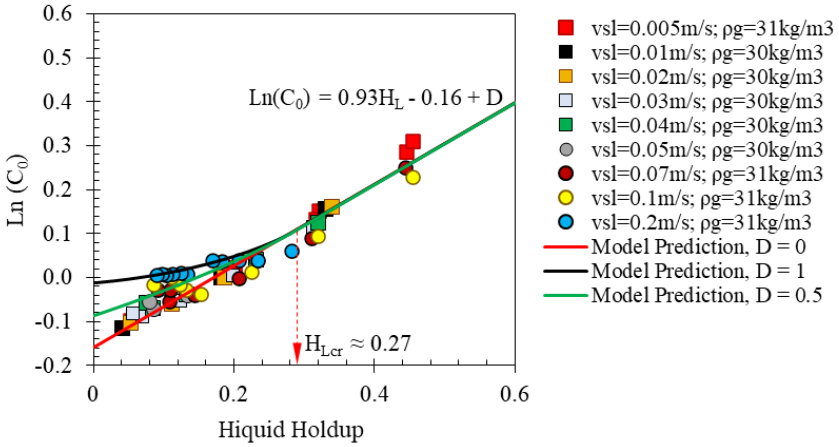

Figure 3-13 The relationship between ln C_0 and H_L for the different liquid flow rates in a 2° upward inclined pipe when gas density is 30 kg/m^3 (data from Soedarmo 2019 and Rodrigues 2018).

3.2.3 New Model for Pressure Gradient Prediction

For the pressure gradient prediction, we adopted the two-fluid model framework (Figure 3-14) that considers the gas and liquid phase frictional pressure losses separately if the liquid phase cannot wet the entire pipe perimeter. This framework is closer to the actual flow behavior in pseudo-slug flow.

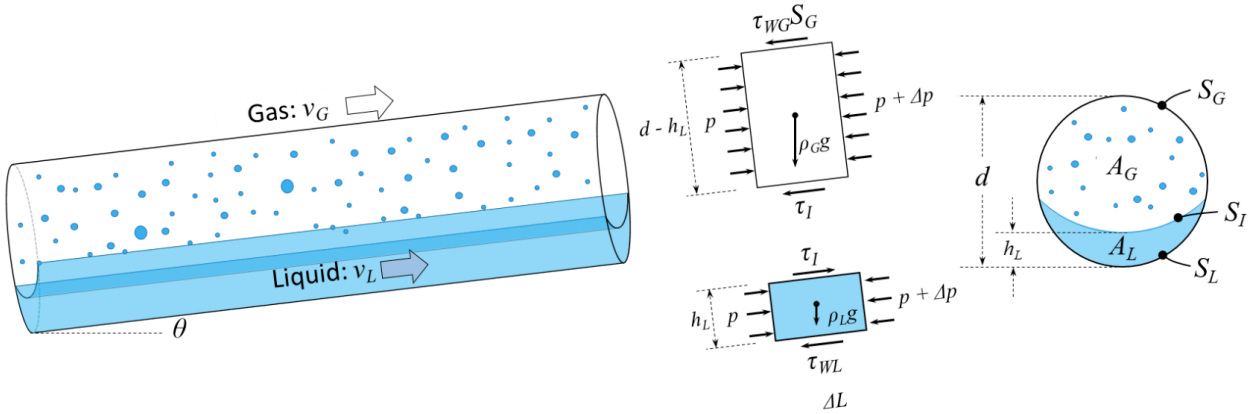

Figure 3-14 Schematic of two-fluid model.

Equations 3-17 and 3-18 are the momentum conservation equations for liquid and gas respectively. Equations 3-19 to 3-21 are the formula for the gas wall shear stress, liquid wall shear stress, and gas-liquid interfacial shear stress, respectively.

$$-\frac{d\overline{P}}{dl}\Big|_L = \overline{\tau}_L \frac{\overline{S}_L}{\overline{A}_L} - \overline{\tau}_I \frac{\overline{S}_I}{\overline{A}_L} + \rho_L \; g \; \sin\theta \tag{3-17}$$

$$-\frac{d\overline{P}}{dl}\Big|_G = \overline{\tau}_G \frac{\overline{S}_G}{\overline{A}_G} + \overline{\tau}_I \frac{\overline{S}_I}{\overline{A}_G} + \rho_G \; g \; \sin\theta \tag{3-18}$$

$$\overline{\tau}_G = f_G \frac{\rho_G \overline{v}_G{}^2}{2} \tag{3-19}$$

$$\overline{\tau}_L = f_L \frac{\rho_L \overline{v}_L{}^2}{2} \tag{3-20}$$

$$\overline{\tau}_I = f_I \frac{\rho_G (\overline{v}_G - \overline{v}_L)\,|\overline{v}_G - \overline{v}_L|}{2} \tag{3-21}$$

The total pressure gradient can be obtained by canceling the interfacial shear stresses in Equations 3-17 and 3-18, and is given by:

$$-\frac{d\overline{P}}{dl} = \frac{\overline{\tau}_L \overline{S}_L + \overline{\tau}_G \overline{S}_G}{\overline{A}_L + \overline{A}_G} + \rho_L \left(\frac{\overline{A}_L}{\overline{A}_L + \overline{A}_G}\right) g \; \sin\theta + \rho_G \left(\frac{\overline{A}_G}{\overline{A}_L + \overline{A}_G}\right) g \; \sin\theta$$

$$= \frac{\overline{\tau}_L \overline{S}_L + \overline{\tau}_G \overline{S}_G}{A_P} + \overline{\rho}_M \; g \; \sin\theta \tag{3-22}$$

Instead of using flat interface configuration (Taitel and Dukler 1976) for the wetted perimeters (S_L and S_G in Figure 3-14) as Soedarmo (2019) assumed for pseudo-slug flow, or annular flow configuration as Pagan et al. (2017) proposed in their model, we propose to use Zhang and Sarica (2011) wetted perimeter correlations, that considers the inclination angle effect. The geometrical parameters in Zhang and Sarica (2011) model assume a double circle interface instead of flat interface. However, it has been noticed that their correlation fails to capture the trend for liquid holdup less than 0.1 approximately (Figure 3-15). The liquid wetted perimeter approaches to annular flow as the liquid holdup reduces below 0.1, which is contradicting with the experimental observation. We proposed another correlation for the liquid wetted perimeter for liquid holdup less than 0.15 (instead of 0.1 to be more conservative), as given in Equation 3-23. The relationship between the dimensionless liquid wetted perimeter and inclination angle for different liquid holdups before and after the correction is shown in Figures 3-16 and 3-17, respectively.

$$S_L = \begin{cases} S_{L\_FI}, \ \theta \leq \frac{\pi}{4} \\ \pi d \left[\left(1 - \frac{S_{L\_FI}}{\pi d}\right) \left(\frac{4\theta}{\pi} - 1\right)^8 + \frac{S_{L\_FI}}{\pi d} \right], \ \theta > \frac{\pi}{4} \end{cases} \tag{3-23}$$

where S_{L_FI} is the liquid wetted perimeter assuming a flat interface as proposed by Taitel and Dukler (1976). The correlation assumes that the liquid wetted perimeter is close to the one for a flat interface for an inclination angle less than 45°, and then gradually changes to the one for annular flow (or uniform distribution) as the inclination angle increases from 45° to 90°. This is consistent with the experimental observation from previous study (Zhu 2019).

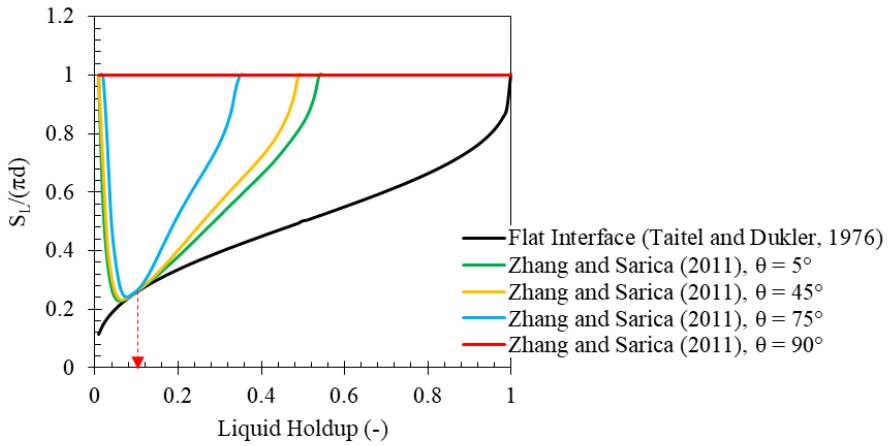

Figure 3-15 Liquid wetted perimeter as a function of liquid holdup for different inclination angles (predicted by Zhang and Sarica 2011 and Taitel and Dukler 1976).

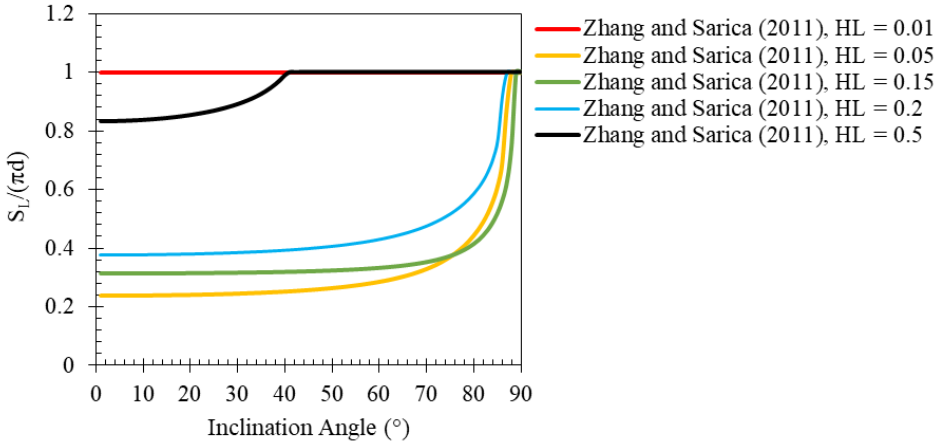

Figure 3-16 Liquid wetted perimeter as a function of inclination angle for different liquid holdup (predicted by Zhang and Sarica 2011).

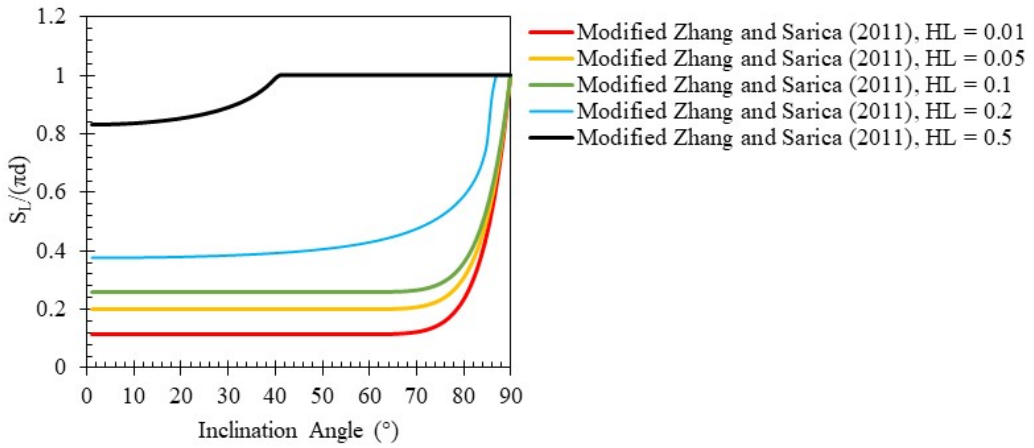

Figure 3-17 Liquid wetted perimeter as a function of inclination angle for different liquid holdup (predicted by the modified Zhang and Sarica 2011).

Unlike segregated flow, the pseudo-slug and churn flow demonstrate an intermittent flow behavior, in which "huge waves" travel intermittently and can lead to additional frictional pressure drops. Besides, the liquid film does not travel continuously at an almost constant velocity as it is in segregated flow, but flows forward and backward due to the opposing forces from the gas phase and gravity. With these considerations, we propose two modifications to the original two-fluid model developed for segregated flow.

The first modification is the addition of the frictional pressure drop in the gas wetted region due to the intermittent "huge waves". We propose to add a multiplying factor in front of the gas wall friction factor developed for single phase gas flow, f_{G_SP}, as show in Equation 3-24.

$$f_{GM} = 2.5\, f_{G\_SP} \tag{3-24}$$

where f_{GM} is the modified gas wall friction factor for pseudo-slug and churn flows, and f_{G_SP} is the gas wall friction factor for single phase flow and can be determined from Colebrook (1939) correlation.

In addition, we propose to modify the average liquid film velocity by considering its intermittent behaviors. The modified average liquid film velocity is given in Equations 3-25 to

3-28. To determine the total pressure gradient, the user can simply replace f_G and $\overline{v}_L$ in Equations 3-19 and 3-21 with the modified f_{GM} and $\overline{v}_{LM}$. All the calculation methods for the rest parameters in Equation 3-22 are the same with the segregated flow.

$$\overline{v}_{LM} = \phi\, \overline{v}_L = \phi\, \frac{v_{SL}}{H_L} \tag{3-25}$$

$$\phi = 11\,(\mu_L - 0.001)^2 + \phi_{1cp} \tag{3-26}$$

$$\phi_{1cp} = \begin{cases} 0.8, & \theta < \frac{\pi}{4} \\ (\phi_{90} - 0.8)\left(\frac{\theta}{\pi/4} - 1\right)^4 + 0.8, & \theta \geq \frac{\pi}{4} \end{cases} \tag{3-27}$$

$$\phi_{90} = \begin{cases} 0.5, & d \leq 0.0508 \\ -904.055(d - 0.0508)^3 + 0.5, & 0.0508 < d < 0.127 \\ 0.1, & d \geq 0.127 \end{cases} \tag{3-28}$$

$\overline{v}_{LM}$ is the corrected average liquid film velocity. The coefficient ϕ accounts for the effects of inclination angle, pipe diameter, and liquid viscosity on the average liquid film velocity. ϕ_{1cp} is the correction factor for fluids with viscosity of 1cp, and ϕ_{90} is the correction factor for fluid flow in vertical pipes. It is hypothesized that the average liquid film velocity reduces as the pipe diameter increases based on the experimental data in vertical pipes (Skopich 2012; Van der Meulen 2012). However, the diameter effects are not obvious for fluid flow in slightly inclined pipes due to less gravity effects based on data from (Alsaadi 2013, 2019). In addition, the coefficient decreases with increasing inclination angle. This might be due to the increase of the gravity effect that increases the amount of liquid film reversal. Furthermore, a higher liquid viscosity results in a higher coefficient (or the average liquid film velocity). This is expected as a higher liquid viscosity can prevent the liquid film from flowing backward due to the high liquid wall friction.

3.3 Model Evaluation

Based on the experimental dataset, the liquid holdup and pressure gradient are noticed to be mainly affected by the following parameters, superficial gas velocity v_{SG}, superficial liquid velocity v_{SL}, inclination angle θ, pipe diameter d, liquid viscosity μ_L, and gas density ρ_G. This section discusses the effect of different parameters on the liquid holdup and pressure gradient respectively, followed by the comparison with other available models.

3.3.1 Parametric Analysis on Liquid Holdup

The increase of gas flow rate decreases the liquid holdup in all experimental studies. The magnitude of the increment of liquid holdup with increasing gas flow rate, however, reduces as the gas flow rate increases. The increase of liquid flow rate increases the liquid holdup and is more obvious at higher v_{SG} values near the transition boundaries between pseudo-slug/churn flow to segregated flow. The following plots shows the effects of the gas and liquid flow rates on the liquid holdup, from different datasets.

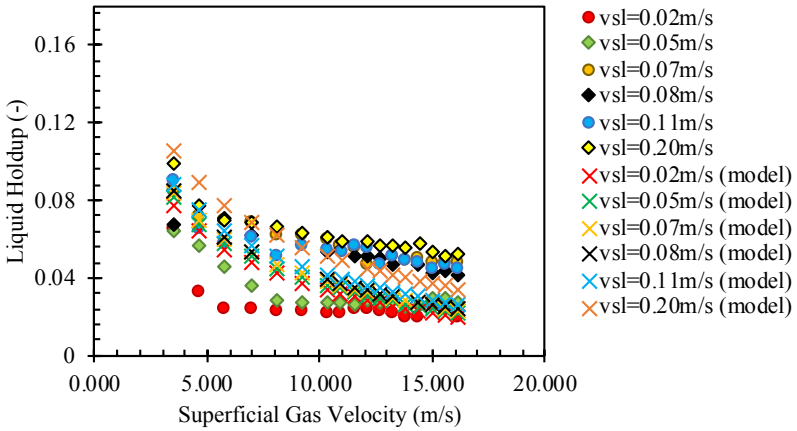

Figure 3-18 Experimentally measured liquid holdup vs. superficial gas velocity and the proposed model prediction (data from Abdulkadir et al. 2019).

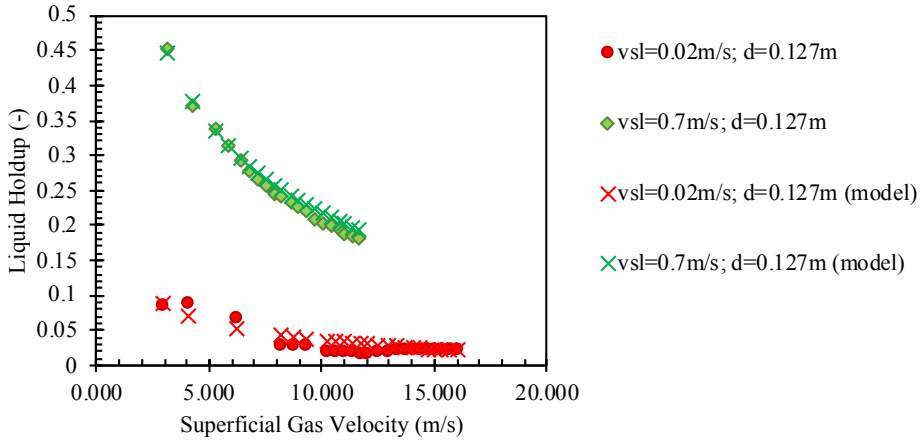

Figure 3-19 Experimentally measured liquid holdup vs. superficial gas velocity and the proposed model prediction (data from van der Meulen 2012).

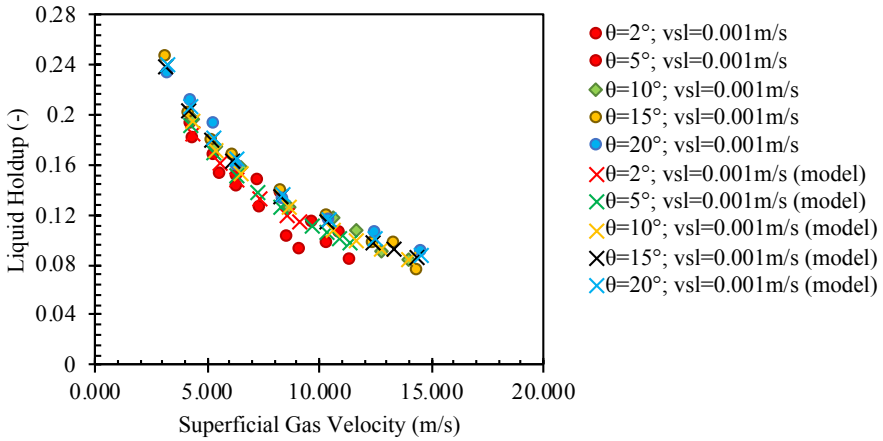

Figure 3-20 Experimentally measured liquid holdup vs. superficial gas velocity and the proposed model prediction (data from Fan 2017).

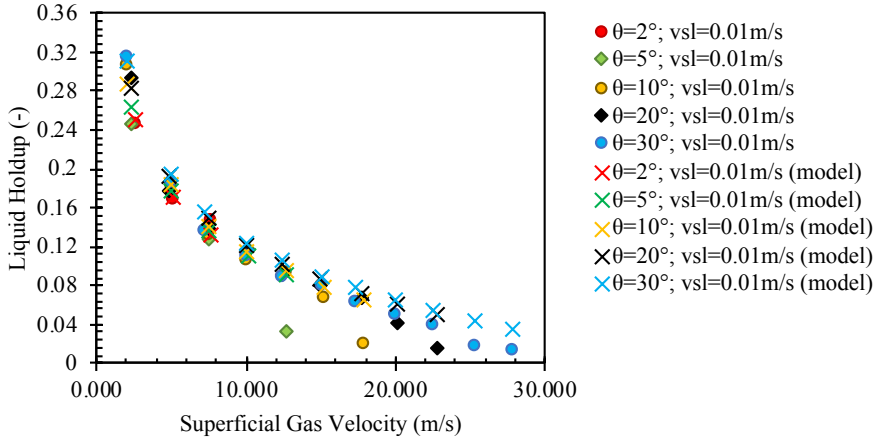

Figure 3-21 Experimentally measured liquid holdup vs. superficial gas velocity and the proposed model prediction (data from Al-Saadi 2013).

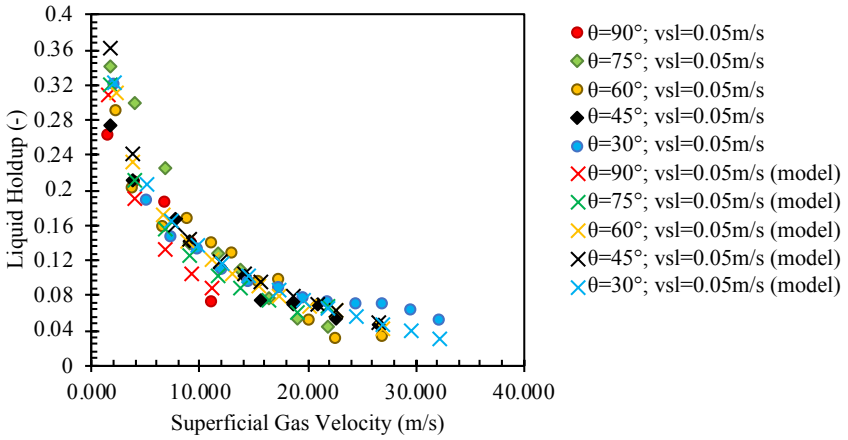

Figure 3-22 Experimentally measured liquid holdup vs. superficial gas velocity and the proposed model prediction (data from Guner 2012).

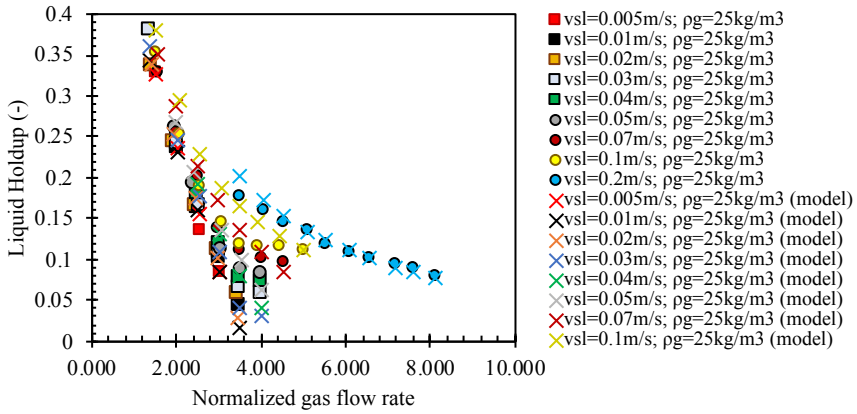

Figure 3-23 Experimentally measured liquid holdup vs. superficial gas velocity and the proposed model prediction (data from Rodrigues 2018 and Soedarmo-HP 2019).

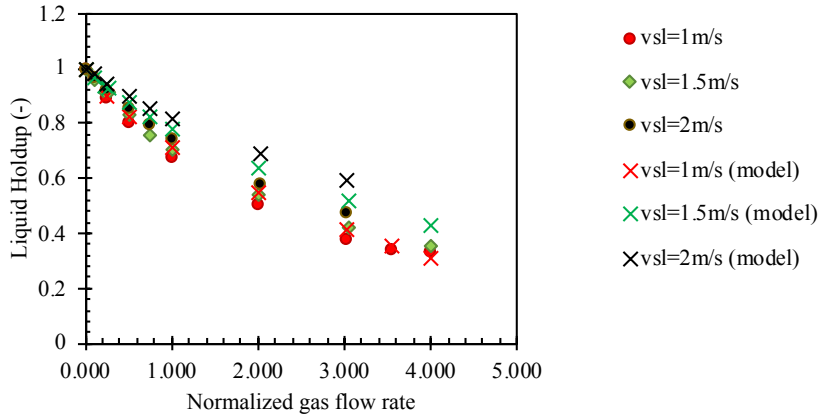

Figure 3-24 Experimentally measured liquid holdup vs. superficial gas velocity and the proposed model prediction (data from Kjølaas et al 2018).

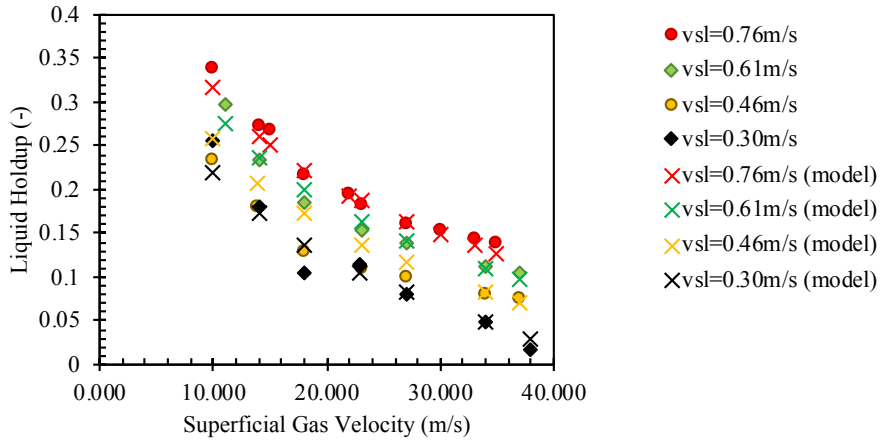

Figure 3-25 Experimentally measured liquid holdup vs. superficial gas velocity and the proposed model prediction (data from Parsi 2015b).

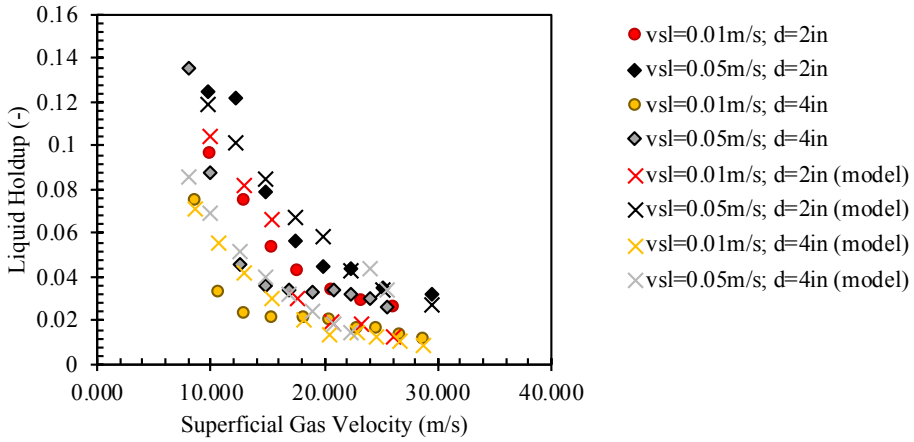

Figure 3-26 Experimentally measured liquid holdup vs superficial gas velocity and the proposed model prediction (data from Skopich 2012).

The experimental data also show that the liquid holdup slightly variates and then decreases with increasing inclination angle from horizontal to vertical. The effect is more noticeable at lower v_{SG} values, as shown in Figures 3-27 and 3-28, data from Zhu (2019) and Soedarmo (2019). As for the diameter, the bigger the diameter the smaller the H_L, as shown in Skopich (2012) (Figure 3-26).

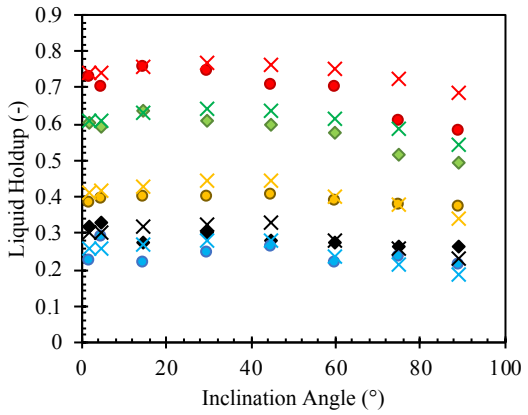

Figure 3-27 Experimentally measued liquid holdup vs inclination angle and the proposed model prediction (data from Zhu 2019, different color represents different gas flow rates).

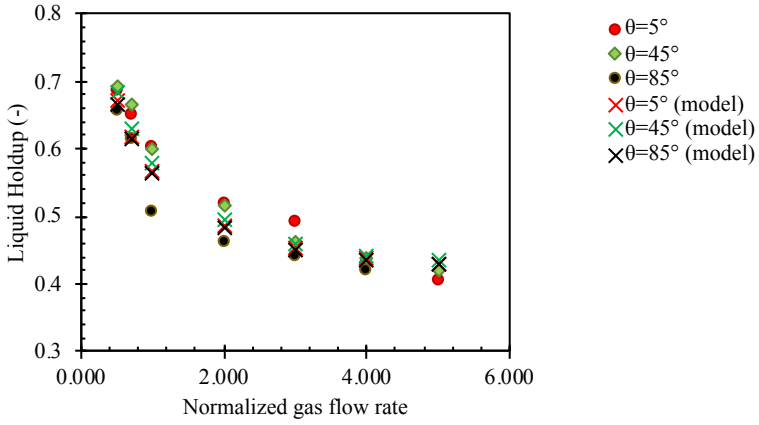

Figure 3-28 Experimentally measured liquid holdup vs superficial gas velocity and the proposed model prediction (data from Soedarmo 2019).

The μ_L is proportional to the liquid holdup. The bigger the μ_L, the liquid holdup is more independent from the v_{SL} effect. On the other hand, for smaller μ_L values, H_L is more sensitive to v_{SL}. It increases with increasing v_{SL} more obviously as it would for high μ_L values (Figures 3-29 to 3-31).

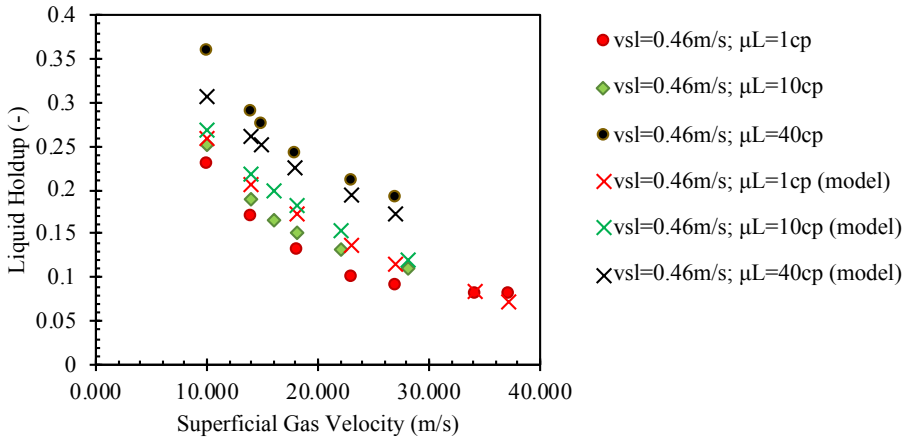

Figure 3-29 Experimentally measured liquid holdup vs superficial gas velocity and the proposed model prediction at $v_{SL} = 0.46$ m/s (data from Parsi 2015a).

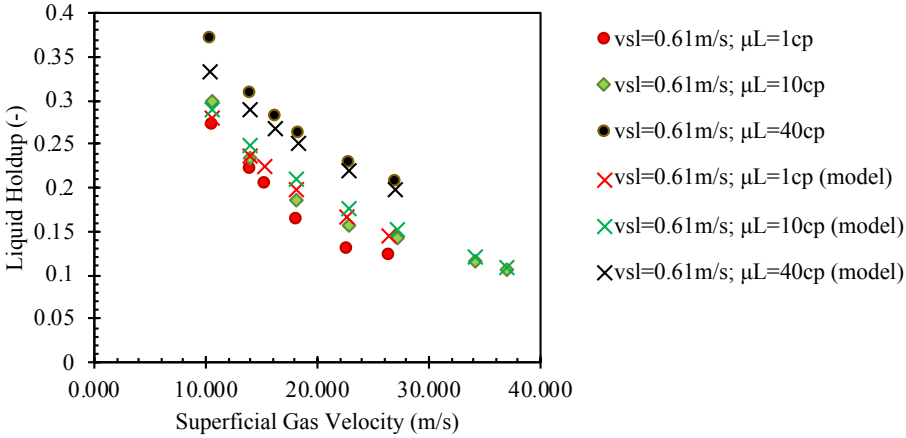

Figure 3-30 Experimentally measured liquid holdup vs superficial gas velocity and the proposed model prediction at $v_{SL} = 0.61$ m/s (data from Parsi 2015a).

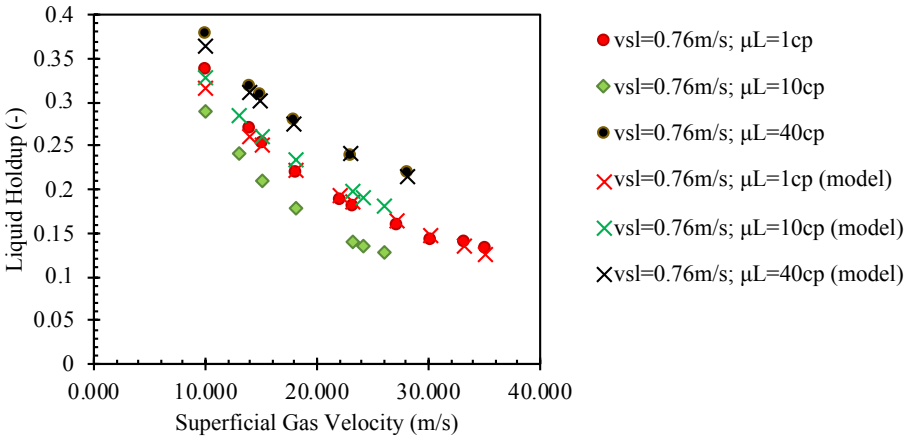

Figure 3-31 Experimentally measured liquid holdup vs superficial gas velocity and the proposed model prediction at $v_{SL} = 0.76$ m/s (data from Parsi 2015a).

The effect of the ρ_G is inversely proportional to H_L as if the ρ_G increases the smaller the H_L will become (Figures 3-32 and 3-33). This is due to the increase of the superficial gas velocity value at which the transition from segregated to intermittent flow occurs as gas density increases (Rastogi and Fan 2020).

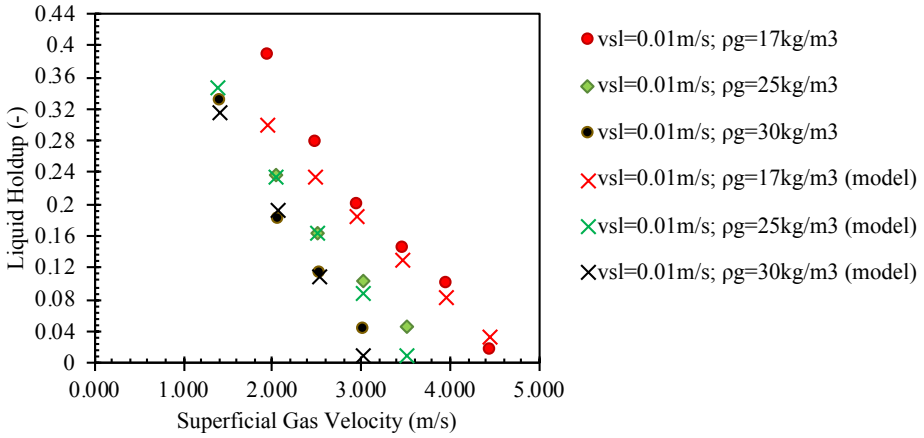

Figure 3-32 Experimentally measured liquid holdup vs superficial gas velocity and the proposed model prediction (data from Rodrigues 2018).

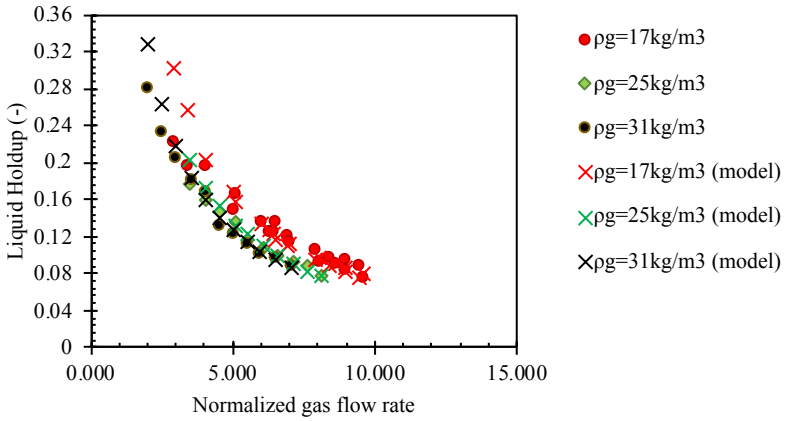

Figure 3-33 Experimentally measured liquid holdup vs superficial gas velocity and the proposed model prediction (data from Soedarmo 2019).

3.3.2 Parametric Analysis on Pressure Gradient

Pressure gradient is mainly composed of two terms, frictional pressure drop that increases with increasing gas flow rate, and the gravitational pressure drop that decreases with increasing gas flow rate. The following Figures show the effects of gas and liquid flow rates on the pressure gradient.

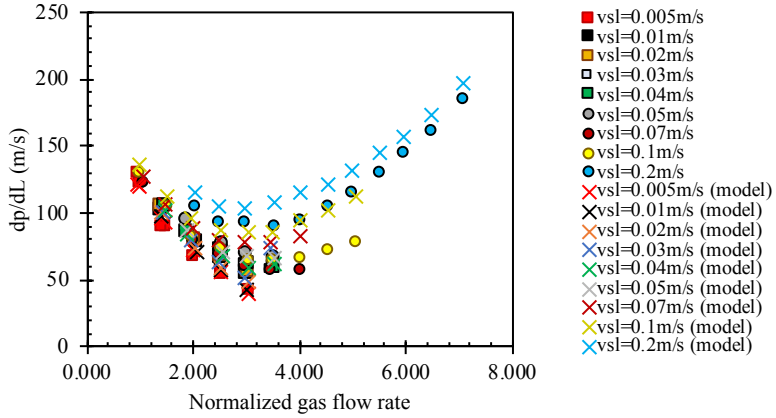

Figure 3-34 Experimentally measured pressure gradient vs. superficial gas velocity and the proposed model prediction (data from Rodrigues 2018 and Soedarmo 2019).

The datasets also show that the increase of inclination angle increases the pressure gradient until the angle reaches near vertical, after which the pressure gradient stays constant or slightly reduced as shown in Figure 3-35 from Zhu (2019). Besides, the bigger the diameter, the smaller pressure gradient as seen in Figure 3-36, data from Skopich (2012). The increase of ρ_G causes decrease in pressure gradient as seen in Figure 3-37, (data from Rodrigues 2018).

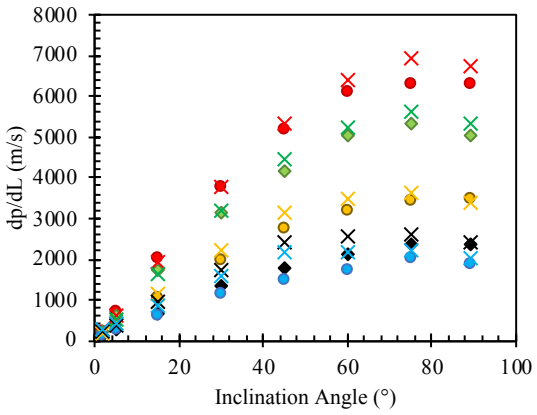

Figure 3-35 Experimentally measured pressure gradient vs inclination angle and the proposed model prediction (data from Zhu 2019, different colors represent different gas flow rates).

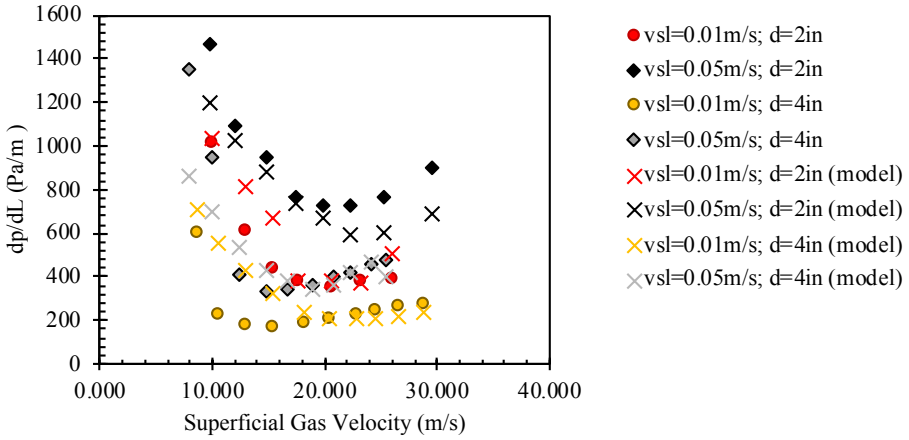

Figure 3-36 Experimentally measured pressure gradient vs superficial gas velocity and the proposed model prediction (data from Skopich 2012).

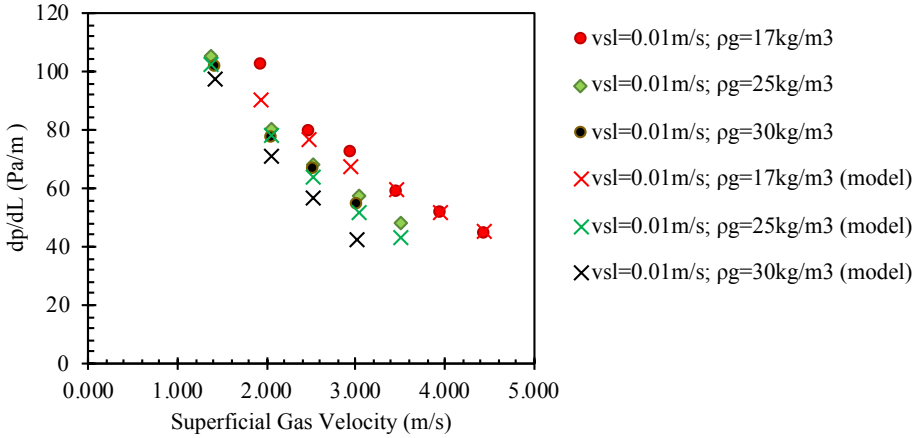

Figure 3-37 Experimentally measured pressure gradient vs superficial gas velocity and the proposed model prediction (data from Rodrigues 2018).

3.3.3 Comparison With Other Models

The following plots show the parity plots for the proposed model, Bhagwat's model. Soedarmo's model, and Pagan's model for both liquid holdup and pressure gradient data.

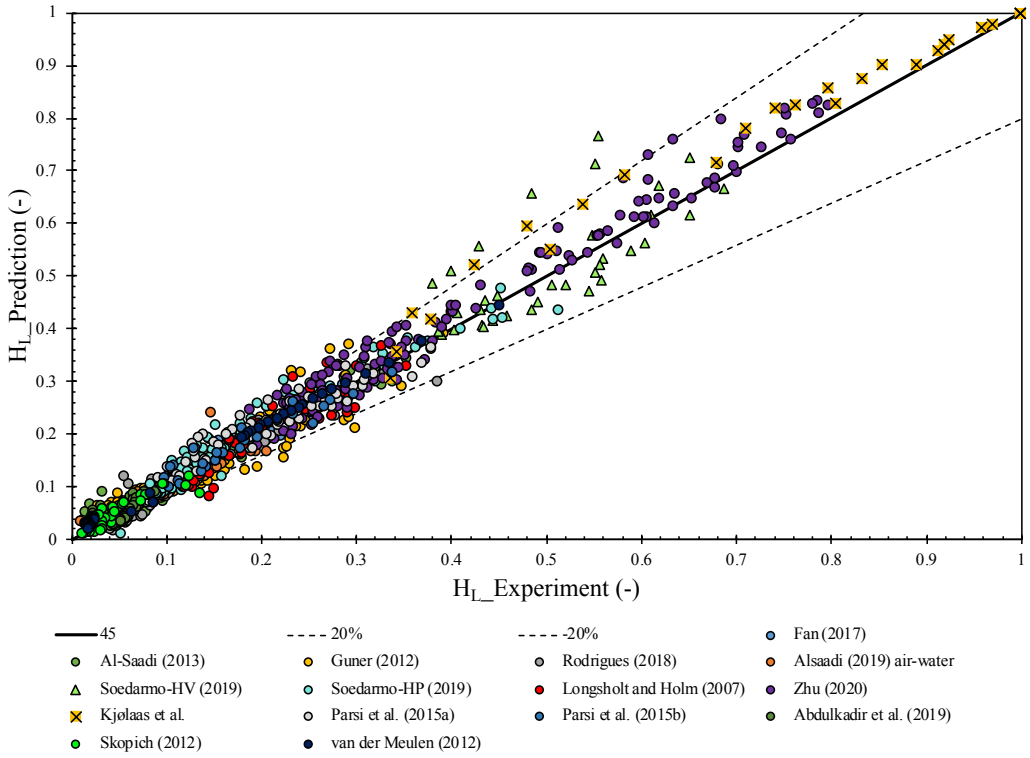

Figure 3-38 Parity plot of the liquid holdup for the proposed model.

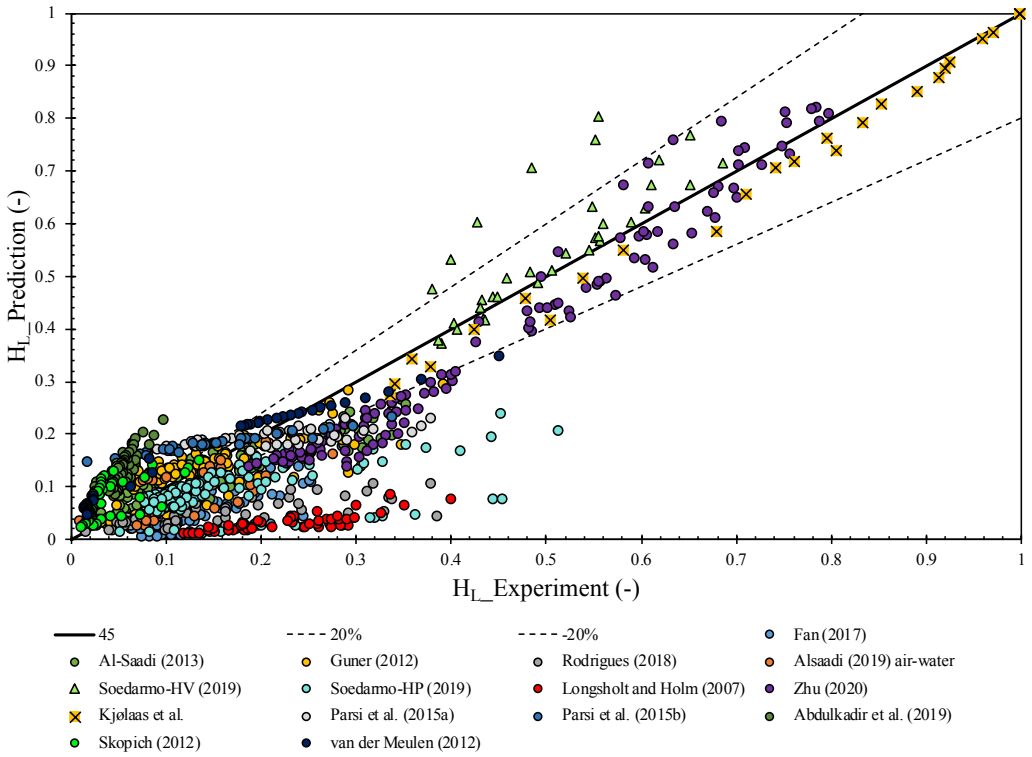

Figure 3-39 Parity plot of the liquid holdup for Bhagwat and Ghajar's (2014) drift flux model.

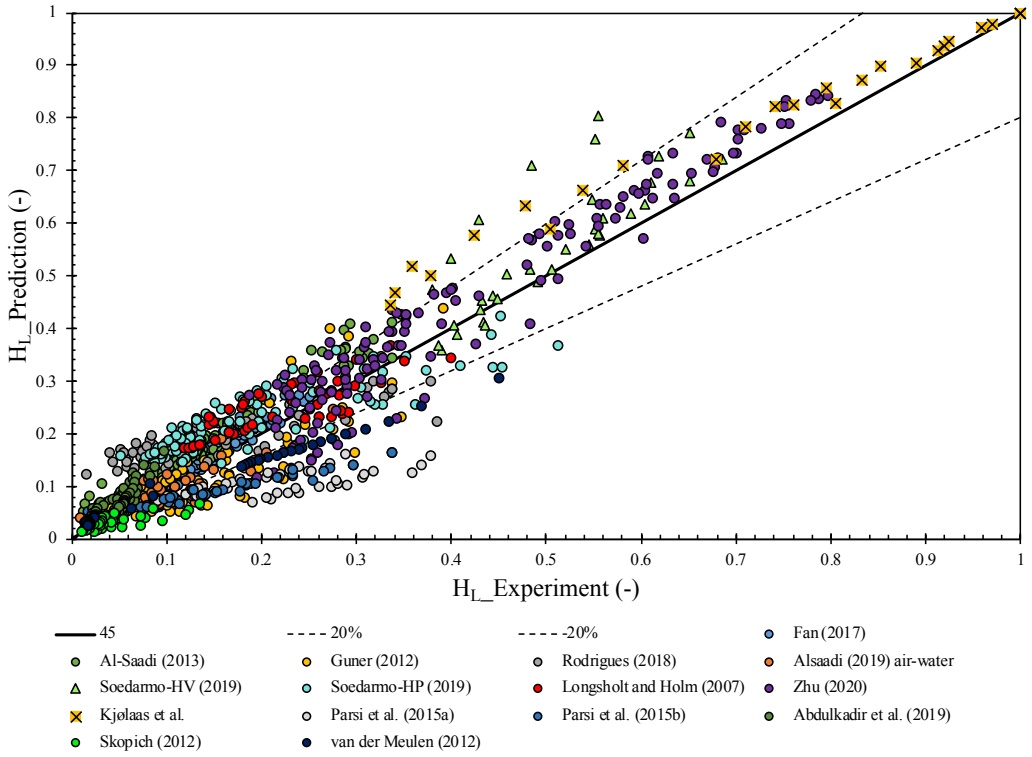

Figure 3-40 Parity plot of the liquid holdup for Soedarmo's (2019) drift flux model.

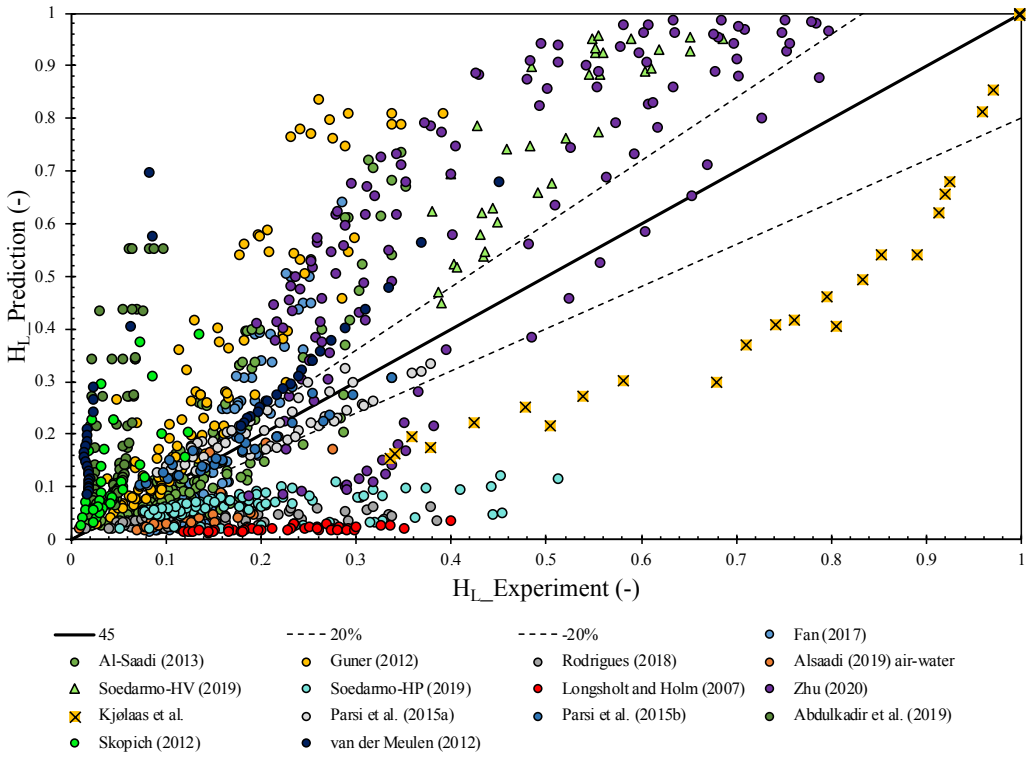

Figure 3-41 Parity plot of the liquid holdup for Pagan's (2017) model.

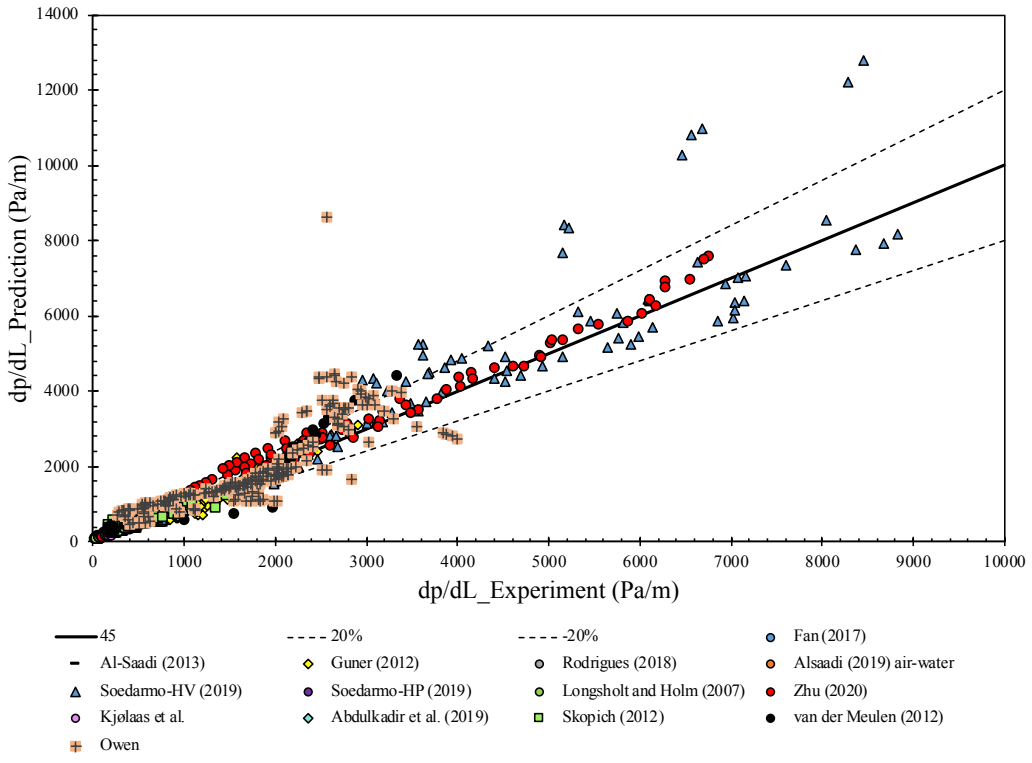

Figure 3-42 Parity plot of the pressure gradient for the proposed model.

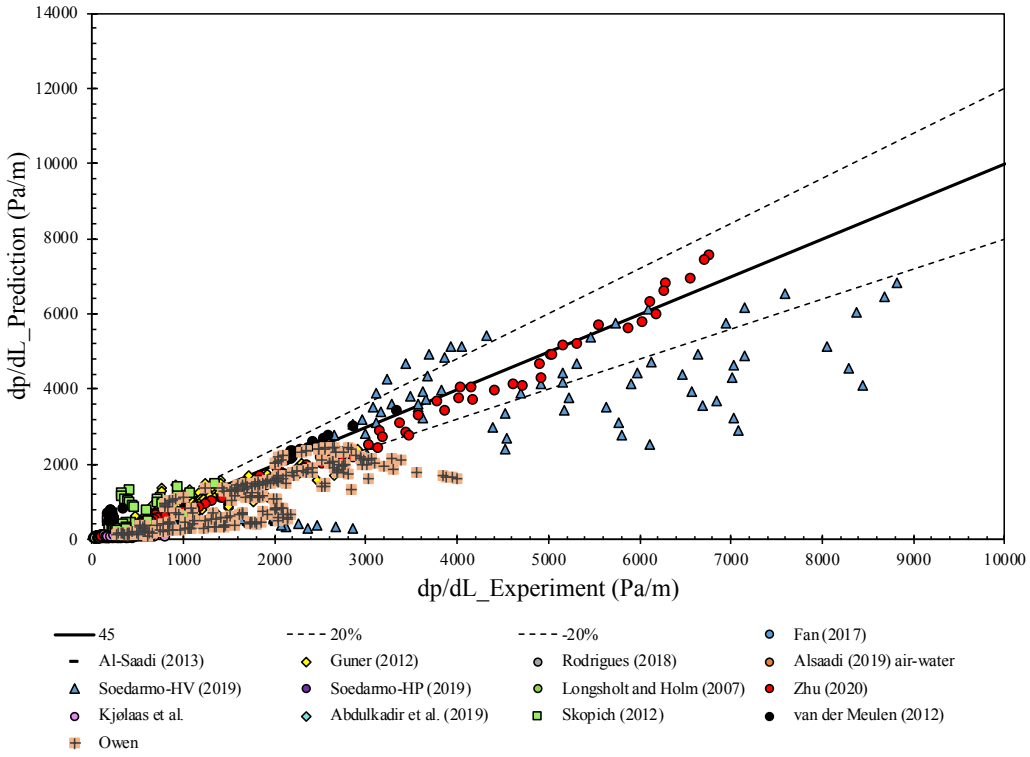

Figure 3-43 Parity plot of the pressure gradient for Bhagwat and Ghajar's (2014) drift flux model.

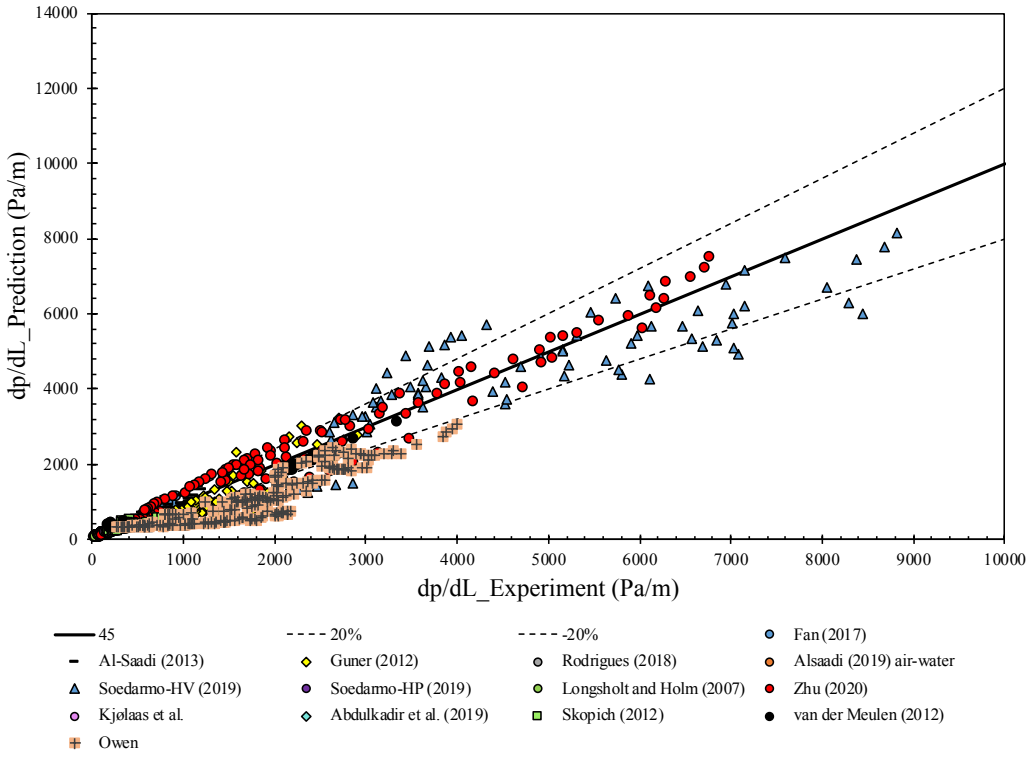

Figure 3-44 Parity plot of the pressure gradient for Soedarmo's (2019) drift flux model.

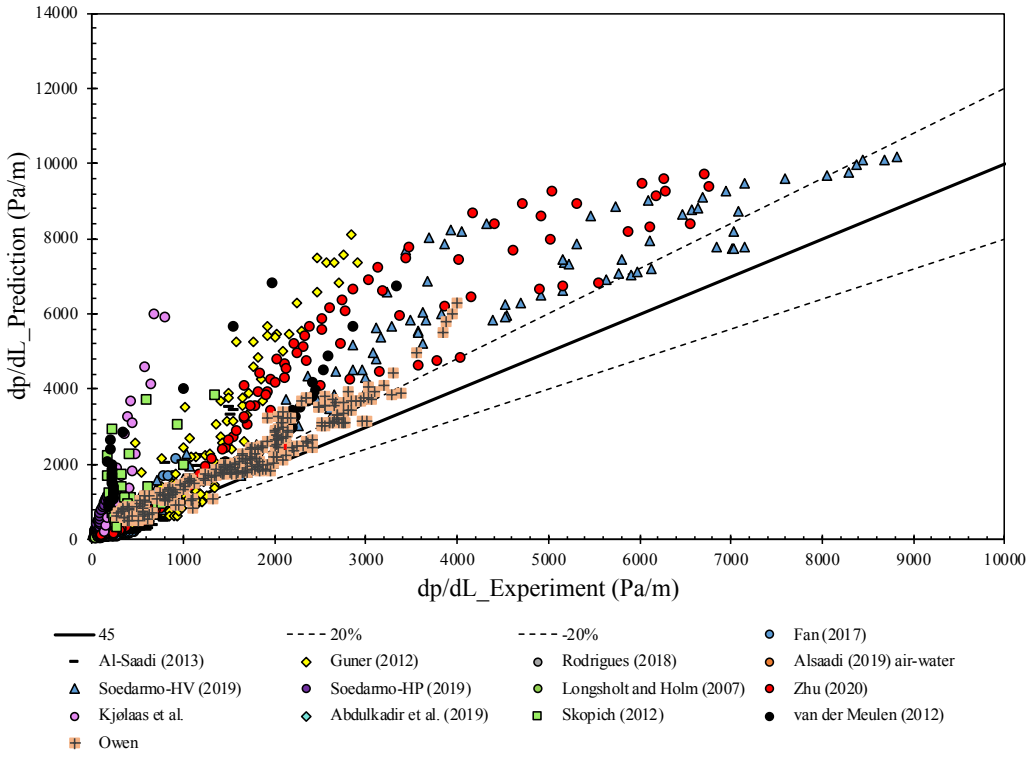

Figure 3-45 Parity plot of the pressure gradient for Pagan's (2017) model.

3.3.4 Statistical Parameters

The average absolute relative error, ε_2, is calculated and shown in Tables 3-2 for liquid holdup and Table 3-3 for pressure gradient predictions, respectively. The equations to calculate the average absolute relative error are given by:

$$e_{ri} = \frac{X_{prediction,i} - X_{measurement,i}}{X_{measurement,i}} \tag{3-28}$$

$$\varepsilon_2 = \frac{1}{N}\sum_{i=1}^{N}|e_{ri}| \tag{3-29}$$

As can be seen that, the new model predicts well for both the liquid holdup and pressure gradient, with average absolute relative errors of 13.99% and 19.10%, respectively. The existing models perform relatively lower than the proposed model by having the closest absolute relative

error to the proposed model equals to 24.16% and 23.62% for the liquid holdup and pressure gradient, respectively.

Table 3-2 Average absolute relative errors for liquid holdup prediction

Data set	Drift Flux Model							Unit Cell	Modified SEG
	Bhagwat and Ghajar (2014)	Bonnecaze et al. (1971)	Shipley et al. (1984)	Gomez et al. (2000)	Tengesdal et al. (1999)	Soedarmo et al. (2018)	New Model	Soedarmo (2019)	Pagan et al. (2017)
Fan (2017)	65.65%	63.62%	75.37%	34.21%	73.38%	10.62%	6.39%	10.62%	56.21%
Alsaadi (2013)	26.84%	111.88%	121.69%	72.35%	70.35%	33.56%	16.31%	33.56%	39.41%
Guner (2012)	38.03%	113.51%	123.16%	75.04%	68.89%	27.30%	18.83%	27.30%	82.07%
Rodrigues (2018)	64.39%	152.36%	179.68%	69.58%	36.96%	74.50%	18.69%	28.87%	69.59%
Alsaadi (2019)	43.93%	120.97%	132.14%	66.19%	72.46%	28.80%	17.18%	28.80%	64.88%
Soedarmo (LPHV) (2019)	6.43%	30.52%	24.46%	45.79%	50.83%	9.66%	4.29%	9.66%	34.82%
Soedarmo (HPLV) (2019)	42.76%	81.22%	95.11%	36.78%	37.91%	45.48%	11.15%	19.29%	61.31%
Longsholt and Holm (2007)	87.94%	29.24%	46.69%	37.12%	46.56%	19.91%	12.45%	13.65%	92.25%
Zhu (2019)	22.08%	7.55%	10.63%	39.54%	37.86%	14.06%	8.07%	14.06%	58.19%
Kjølaas et al. (2018)	6.02%	4.58%	4.92%	5.20%	9.35%	13.16%	7.85%	93.27%	37.46%
Parsi et al. (2015a)	28.36%	31.39%	32.05%	27.57%	75.88%	47.36%	11.59%	47.36%	16.12%
Parsi et al. (2015b)	61.69%	78.00%	80.85%	54.78%	72.95%	44.36%	10.02%	44.35%	27.34%
Abdulkadir et al. (2019)	134.46%	398.44%	428.40%	260.91%	31.09%	29.15%	29.21%	32.76%	283.80%
Skopich (2012)	94.86%	455.72%	478.49%	319.09%	50.47%	30.59%	25.99%	30.61%	212.58%
van der Meulen (2012)	97.22%	424.45%	452.68%	293.34%	38.30%	35.74%	21.79%	35.04%	368.67%
Total	52.03%	122.75%	134.35%	84.01%	53.84%	29.42%	13.99%	24.16%	89.47%

Table 3-3 Average absolute relative errors for pressure gradient prediction

Data set	Drift Flux Model						Unit Cell	Modified SEG	
	Bhagwat and Ghajar (2014)	Bonnecaze et al. (1971)	Shipley et al. (1984)	Gomez et al. (2000)	Tengesdal et al. (1999)	Soedarmo et al. (2018)	Soedarmo (2019)	Pagan et al. (2017)	New Model
Fan (2017)	75.41%	22.68%	25.25%	29.14%	80.14%	19.48%	19.65%	52.63%	16.8%
Alsaadi (2013)	48.86%	25.98%	25.64%	35.63%	81.93%	23.87%	39.25%	38.39%	25.3%
Guner (2012)	23.17%	69.85%	80.16%	46.16%	71.01%	24.09%	209.85%	84.80%	21.37%
Rodrigues (2018)	71.95%	14.50%	21.50%	36.11%	53.10%	12.04%	33.16%	69.74%	7.67%
Alsaadi (2019)	57.98%	16.37%	19.47%	25.88%	82.59%	30.41%	62.56%	41.46%	14.91%
Soedarmo (LPHV) (2019)	36.42%	53.79%	49.85%	63.96%	67.32%	21.15%	223.74%	44.05%	16.79%
Soedarmo (HPLV) (2019)	65.57%	24.81%	26.99%	44.92%	59.40%	15.25%	40.32%	284.77%	12.82%
Longsholt and Holm (2007)	81.37%	26.41%	34.94%	38.08%	45.62%	16.44%	30.82%	55.61%	15.41%
Zhu (2019)	21.52%	11.59%	14.74%	38.58%	37.72%	11.93%	18.58%	57.66%	9.02%
Kjølaas et al. (2018)	82.37%	81.42%	81.62%	82.43	82.73%	15.49%	99.03%	335.27%	10.53%
Skopich (2012)	70.09%	354.76%	374.73%	242.68%	56.50%	30.69%	2812.55%	218.27%	24.58%
van der Meulen (2012)	73.48%	344.89%	368.59%	237.88%	35.41%	29.30%	7148.87%	303.30%	23.09%
Owen (1986)	43.27%	85.39%	102.35%	61.85%	60.89%	40.68%	1261.13%	69.08%	29.63%
Total	54.27%	59.49%	65.28%	56.38%	63.95%	23.62%	1021.3%	91.44%	19.10%

CHAPTER 4
SUMMARY AND RECOMMENDATIONS

A simplified unified hydraulic model for pseudo-slug and churn flows was developed based on experimental studies that covered different parameters in different ranges of values. The experimental dataset was taken from sixteen experimental studies, ten of which are studies on pseudo-slug flow pattern and six on churn flow pattern. The new model predicts the liquid holdup using the drift flux model with new correlations for the drift velocity and the flow distribution coefficient. The drift velocity correlation was developed based on the experimental study from Gokcal et al. (2009), who studied the effects of liquid viscosity and inclination angle on the drift velocity. The flow distribution coefficient is then back calculated using the drift velocity predicted from the new model, and the measured liquid holdup using the drift flux model equation. The development of the distribution coefficient correlation was based on the back calculated values, which showed clear trends with different parameters. The predicted liquid holdup was employed in the pressure gradient calculations based on the two-fluid model framework with modifications on gas and liquid shear stresses considering the oscillation nature of the intermittent flow.

The developed model in this study captures the effects of inclination angle, gas and liquid flow rates, and fluid properties, such as liquid viscosity and gas density. The inclination angle ranges from horizontal to vertical with the majority of the data lies in the vertical inclination and near horizontal and the rest of the data points lies between 5° and 85° in an almost even distribution. The pipe diameter values in the dataset start from 0.032 m to 0.189 m with the majority of data below 0.1 m. In most of current experimental studies, the liquid

phase used is water and few of them used oil due to the practicality and ease to use water over other higher viscous fluids. By including more experimental studies in the future on pseudo-slug and churn flow patterns that especially cover wider range of parameters, the modeling work could be more improved and be more representative to the real-world situation.

REFERENCES

Abdulkadir, M., Mbalisigwe, U.P., Zhao, D., Hernandez-Perez, V., Azzopardi, B.J., and Tahir, S. 2019. Characteristics of churn and annular flows in a large diameter vertical riser. *International Journal of Multiphase Flow* , Vol. **113**, 250-263. https://doi.org/10.1016/j.ijmultiphaseflow.2019.01.013.

Abduvayt, P., Manabe, R., and Arihara, N. 2003. Effects of Pressure and Pipe Diameter on Gas-Liquid Two-Phase Flow Behavior in Pipelines. Paper presented at the SPE Annual Technical Conference and Exhibition, Denver, Colorado, USA . https://doi.org/10.2118/84229-MS.

Alsaadi, Y. 2013. Liquid Loading in Highly Deviated Gas Wells. MSc thesis, University of Tulsa, Tulsa, OK.

Alsaadi, Y. 2019. Low liquid loading two-phase and three-phase flows in slightly upward inclined pipes. PhD dissertation, University of Tulsa, Tulsa, OK.

Alsaadi, Y., Pereyra, E., Torres, C., and Sarica, C. 2015. Liquid Loading of Highly Deviated Gas Wells from 60° to 88°. Paper presented at the SPE Annual Technical Conference and Exhibition, Houston, Texas, USA. https://doi.org/10.2118/174852-MS.

Alves, M. V. C. 2014. Modelagem numérica do escoamento transiente churn-anular em tubulações verticais e sua aplicação na simulação de carga de líquido em poços de gás. Doctorate thesis. Universidade Federal de Santa Catarina, Centro Tecnológico, Programa de Pós-Graduação em Engenharia Mecânica, Florianópolis. https://repositorio.ufsc.br/xmlui/handle/123456789/129372.

Amaravadi, S., Minami, Kazuioshi., and Ovadia, S. 1998. Two-Phase Zero-Net Liquid Flow in Upward Inclined Pipes: Experiment and Modeling. *SPE J.* Vol. **3,** 253–260. https://doi.org/10.2118/50974-PA.

Arabi, A., Salhi, Y., Zenati Y., Si-Ahmed, E.K., and Legrand, J. 2020. On Gas-Liquid Intermittent Flow in a Horizontal Pipe: Influence of Sub-Regime on Slug Frequency. *Chemical Engineering Science,* Vol. **211,** 115251. https://doi.org/10.1016/j.ces.2019.115251.

Arellano, Y., Hunt, A., Haas, O., and Ma, L. 2020. On the Life and Habits of Gas-Core Slugs: Characterisation of an Intermittent Horizontal Two-Phase Flow. *Journal of Natural Gas Science and Engineering,* Vol. **82,** 103475. https://doi.org/10.1016/j.jngse.2020.103475.

Barnea, D., Shoham, O., Taitel, Y., and Dukler, A.E. 1980. Flow Pattern Transition for Gas-Liquid Flow in Horizontal and Inclined Pipes. Comparison of experimental data with theory. *International Journal of Multiphase Flow* **6** (1): 217–225. https://doi.org/10.1016/0301-9322(80)90012-9.

Bendiksen K. and Espedal, M. 1992. Onset of Slugging in Horizontal Gas-Liquid Pipe Flow. *International Journal of Multiphase Flow* **18** (2): 237–247. https://doi.org/10.1016/0301-9322(92)90086-V.

Bendiksen, K.H. 1984. An Experimental Investigation of the Motion of Long Bubbles in Inclined Tubes. *International Journal of Multiphase Flow* **10** (4): 467–483. https://doi.org/10.1016/0301-9322(84)90057-0.

Bhagwat, S.M. and Ghajar, A. J. 2014. A Flow Pattern Independent Drift Flux Model Based Void Fraction Correlation for a Wide Range of Gas–Liquid Two Phase Flow. *International Journal of Multiphase Flow,* Vol. **59**, 186–205. https://doi.org/10.1016/j.ijmultiphaseflow.2013.11.001.

Benjamin, T.B. 1968. Gravity Currents and Related Phenomena. *Journal of Fluid Mechanics,* **31** (2): 209-248. https://doi.org/10.1017/S0022112068000133.

Butterworth, D. and Pulling, D. J. 1972. A Visual Study of Mechanisms in Horizontal, Annular, Air-Water Flow. *Volume 2556 of AERE memorandum.* Atomic Energy Research Establishment.

Choi, J., Pereyra, E., Sarica, C., Park C., and Kang, J.M. 2012. An Efficient Drift-Flux Closure Relationship to Estimate Liquid Holdups of Gas-Liquid Two-Phase Flow in Pipes. *Energies* **5** (12): 5294-5306. https://doi.org/10.3390/en5125294.

Chokshi, R.N. 1994. Prediction of Pressure Drop and Liquid Holdup in Vertical Two-Phase Flow Through Large Diameter Tubing. PhD dissertation, University of Tulsa, Tulsa, OK.

Colebrook, C.F. 1939. Turbulent Flow in Pipes, With Particular Reference to the Transition Region Between the Smooth And Rough Pipe Laws. *Journal of the Institution of Civil Engineers* **11** (4): 133–156. https://doi.org/10.1680/ijoti.1939.13150.

Collignon, M., Mazzini, A., Schmid, D.W., and Lupi, M. 2018. Modelling Fluid Flow in Active Clastic Piercements: Challenges and Approaches. *Marine and Petroleum Geology,* Vol. **90**, 157–172. https://doi.org/10.1016/j.marpetgeo.2017.09.033.

Danielson, T.J. and Fan, Y. 2009. Relationship between mixture and two-fluid models. BHR-2009-J3. 14th International Conference on Multiphase Production Technology.

Dasgupta, A., Chandraker, D.K., Kshirasagar, S., Raghavendra Reddy, B., Rajalakshmi, R., Nayak, A.K., Walker, S.P., Vijayan, P.K., and Hewitt, G.F. 2017. Experimental Investigation on Dominant Waves in Upward Air-Water Two-Phase Flow in Churn and Annular Regime. *Experimental Thermal and Fluid Science,* Vol. **81**, 147–163. https://doi.org/10.1016/j.expthermflusci.2016.10.012.

Davies, R.M. and Taylor, G.I. 1950. The mechanics of large bubbles rising through extended liquids and through liquids in tubes. Proceedings of the Royal Society of London. Series A, Mathematical and Physical Sciences **200** (1062): 375–390. https://doi/10.1098/rspa.1950.0023.

De Leebeeck, A. 2010. A Roll Wave and Slug Tracking Scheme for Gas-Liquid Pipe Flow. Doctarate Thesis. NTNU. http://hdl.handle.net/11250/234136.

Dumitrescu, D.T. 1943. Strömung an Einer Luftblase Im Senkrechten Rohr. *ZAMM Z Angew Math Mech,* Vol. **23**, 139-149. https://doi.org/10.1002/zamm.19430230303.

Ekinci, S. 2015. Pipe Inclination Effects on Slug Flow Characteristics of High Viscosity Oil-Gas Two-Phase Flow. MSc thesis, University of Tulsa, Tulsa, OK.

Fabre, J. 1994. Advancements in Two-Phase Slug Flow Modeling. Presented at University of Tulsa Centennial Petroleum Engineering Symposium, Tulsa, Oklahoma. https://doi.org/10.2118/27961-MS.

Fabre, J. and Line, A. 1992. Modeling of Two-Phase Slug Flow. *Annual Review of Fluid Mechanics,* Vol. **24**, 21-46. https://doi:10.1146/annurev.fl.24.010192.000321.

Fan, Y. 2017. A Study of the Onset of Liquid Accumulation and Pseudo-slug Flow Chracterization. PhD dissertation, University of Tulsa, Tulsa, OK.

Fan, Y., Pereyra, E., and Sarica, C. 2020. Experimental study of pseudo-slug flow in upward inclined pipes. *Journal of Natural Gas Science and Engineering,* Vol. **75**, 103147. https://doi.org/10.1016/j.jngse.2020.103147.

Fan, Y., Pereyra, E., Sarica, C., Schleicher, E., and Hampel, U. 2019. Analysis of Flow Pattern Transition From Segregated to Slug Flow in Upward Inclined Pipes. *International Journal of Multiphase Flow,* Vol. **115**, 19–39. https://doi.org/10.1016/j.ijmultiphaseflow.2019.03.021.

França, F. and Lahey, R.T. 1992. The Use of Drift-Flux Techniques for the Analysis of Horizontal Two-Phase Flows. *International Journal of Multiphase Flow* **18** (6): 787–801. https://doi.org/10.1016/0301-9322(92)90059-P.

Gokcal, B., Al-Sarkhi, A. S., and Sarica, C. 2009. Effects of High Oil Viscosity on Drift Velocity for Horizontal and Upward Inclined Pipes. *SPE Proj Fac & Const* **4** (02): 32–40. https://doi.org/10.2118/115342-PA.

Gomez, L. E., Shoham, Ovadia, Schmidt, Zelimir, Chokshi, R. N., and Northug. 2000. Unified Mechanistic Model for Steady-State Two-Phase Flow: Horizontal to Vertical Upward Flow. *SPE J.* **5** (03): 339–350. https://doi.org/10.2118/65705-PA.

Greskovich, E.J. and Cooper, W.T. 1975. Correlation and Prediction of Gas-Liquid Holdups in Inclined Upflows. *AIChE J.* **21** (6): 1189-1192. https://doi.org/10.1002/aic.690210619.

Guner, M. 2012. Liquid Loading of Gas Wells with Deviations from 0° to 45°. MSc thesis, University of Tulsa, Tulsa, OK.

Hibiki T, and Ishii, M. 2003. One-Dimensional Drift-Flux Model and Constitutive Equations for Relative Motion Between Phases in Various Two-Phase Flow Regimes. *International*

Journal of Heat and Mass Transfer **46** (25): 4935–4948. https://doi.org/10.1016/S0017-9310(03)00322-3.

Hunt, A., Pendleton, J., and Ladam, Y. 2004. Visualisation of Two-Phase Gas-Liquid Pipe Flows Using Electrical Capacitance Tomography. *Proceedings of the ASME 7th Biennial Conference on Engineering Systems Design and Analysis,* Vol. **1**, 491–495. https://doi.org/10.1115/ESDA2004-58396.

Ishii, M. 1977. One-Dimensional Drift-Flux Model and Constitutive Equations for Relative Motion Between Phases in Various Two Phase Flow Regimes. Technical Report. Argonne National Laboratory. https://doi.org/10.2172/6871478.

Jayanti, S. and Brauner, N. 1994. Churn Flow. *Multiphase Science and Technology* **8** (1-4): 471-521. https://doi.org/10.1615/MultScienTechn.v8.i1-4.90.

Kataoka, I. and Ishii, M. 1987. Drift Flux Model for Large Diameter Pipe and New Correlation for Pool Void Fraction. *International Journal of Heat and Mass Transfer* **30** (9): 1927–1939. https://doi.org/10.1016/0017-9310(87)90251-1.

Kesana, N.R., Parsi, M., Vieira, R.E., Azzopardi, A., Schleicher, E., McLaury, B.S., Shirazi, S.A., and Hampel, U. 2017. Visualization of Gas-Liquid Multiphase Pseudo-Slug Flow Using Wire-Mesh Sensor. *Journal of Natural Gas Science and Engineering,* Vol. **46**, 477–490. https://doi.org/10.1016/j.jngse.2017.08.010.

Kjølaas, J., Smith, I. E., and Brekken, C. 2018. Pseudo Slug Flow in Viscous Oil Systems - Experiments And Modelling with Ledaflow. Paper presented at the 11th North American Conference on Multiphase Production Technology, Banff, Canada.

Kokal, S.L. and Stanislav, J.F. 1989. An Experimental Study of Two-Phase Flow in Slightly Inclined Pipes – i. Flow Patterns. *Chemical Engineering Science* **44** (3): 665–679. https://doi.org/10.1016/0009-2509(89)85042-0.

Lam Loh, W., Hernandez-Perez, V., Tam, N.D., Wan, T.T., Yuqiao, Z., and Premanadhan, V.K. 2016. Experimental Study of the Effect of Pressure and Gas Density on the Transition From Stratified to Slug Flow in a Horizontal Pipe. *International Journal of Multiphase Flow*, Vol. **85**, 196-208. https://doi.org/10.1016/j.ijmultiphaseflow.2016.06.005.

Langsholt, M., and Holm, H. 2007. Liquid Accumulation in Gas-Condensate Pipelines – An Experimental Study. Paper presented at the 13th International Conference on Multiphase Production Technology, Edinburgh, UK.

Lin, P.Y. and Hanratty, T.J. 1987. Effect of Pipe Diameter on Flow Patterns for Air-Water Flow in Horizontal Pipes. *International Journal of Multiphase Flow* **13** (4): 549–563. https://doi.org/10.1016/0301-9322(87)90021-8.

Maley, J. 1997. Slug flow Characteristics and Corrosion Rates in Inclined High Pressure Multiphase Flow Pipes. MSc thesis, Ohio University, Athens, OH.

Nicholson, M.K., Aziz, K., and Gregory, G.A. 1978. Intermittent Two Phase Flow in Horizontal Pipes: Predictive Models. *Canadian Journal of Chem Eng* **56** (6): 653–663. https://doi.org/10.1002/cjce.5450560601.

Omebere-Iyari, N.K. and Azzopardi, B.J. 2007. A Study of Flow Patterns for Gas/Liquid Flow in Small Diameter Tubes. *Chemical Engineering Research and Design* **85** (2): 180–192. https://doi.org/10.1205/cherd05059.

Owen, D.G. 1986. An Experimental and Theoretical Analysis of Equilibrium Annular Flows. PhD dissertation, University of Birmingham, Birmingham, United Kingdom.

Pagan, E., Williams, W.C., Kam, S., and Waltrich, P.J. 2017. A Simplified Model for Churn and Annular Flow Regimes in Small- And Large-Diameter Pipes. *Chemical Engineering Science,* Vol. **162**, 309–321. https://doi.org/10.1016/j.ces.2016.12.059.

Parsi, M., Azzopardi, B.J., Al-Sarkhi, A., Kesana, N.R., Vieira, R.E., Torres, C.F., McLaury, B.S., Shirazi, S.A., Schleicher, E., and Hampel, U. 2017. Do Huge Waves Exist in Horizontal Gas-Liquid Pipe Flow? *International Journal of Multiphase Flow,* Vol. **96**, 1-23. https://doi.org/10.1016/j.ijmultiphaseflow.2017.06.007.

Parsi, M., Vieira, R.E., Torres, C.F., Kesana, N.R., McLaury, B.S., Shirazi, S.A., Schleicher, E., and Hampel, U. 2015a. On The Effect of Liquid Viscosity on Interfacial Structures Within Churn Flow: Experimental Study Using Wire Mesh Sensor. *Chemical Engineering Science,* Vol. **130**, 221–238. https://doi.org/10.1016/j.ces.2015.03.033.

Parsi, M., Vieira, R.E., Torres, C.F., Kesana, N.R., McLaury, B.S., Shirazi, S.A., Schleicher, E., and Hampel, U. 2015b. Experimental Investigation of Interfacial Structures Within Churn Flow Using a Dual Wire-Mesh Sensor. International *Journal of Multiphase Flow,* Vol. **73**, 155–170. https://doi.org/10.1016/j.ijmultiphaseflow.2015.03.019.

Rastogi, A., and Fan, Y. 2019. Experimental Investigation and Modeling of Onset of Liquid Accumulation in Large- Diameter Deviated Gas Wells." Paper presented at the SPE Annual Technical Conference and Exhibition, Calgary, Alberta, Canada. https://doi.org/10.2118/196130-MS.

Rastogi, A. and Fan, Y., 2022. Machine Learning Augmented Two-Fluid Model for Segregated Flow. *Fluids* **7** (1): 12. https://doi.org/10.3390/fluids7010012.

Rodrigues, H.T. 2018. Pressure Effects on Low-Liquid Loading Two-Phase Flow in Near-Horizontal Upward Inclined Pipes. PhD dissertation, University of Tulsa, Tulsa, OK.

Rodrigues, H. T., Pereyra, E., and Sarica, C. 2019. Pressure Effects on Low-Liquid-Loading Oil/Gas Flow in Slightly Upward Inclined Pipes: Flow Pattern, Pressure Gradient, and Liquid Holdup. *SPE J.* Vol. **24**, 2221–2238. https://doi.org/10.2118/191543-PA.

Sekoguchi, K. and Mori, K. 1997. New Development of Experimental Study on Interfacial Structure in Gas-Liquid Two-Phase Flow. 4th World Conference on Experimental Heat Transfer, Fluid Mechanics and Thermodynamics, Brussels.

Shi, H., Holmes, J., Durlofsky, L.J., Aziz, K., Díaz, L.R., Alkaya, B., and Oddie, G.M. 2005. Drift-Flux Modeling of Two-Phase Flow in Wellbores. *Spe Journal,* Vol. **10**, 24-33.

Shipley, D.G. 1984. Two Phase Flow in Large Diameter Pipes. *Chem. Eng. Sci*. **39** (1): 163–165. https://doi.org/10.1016/0009-2509(84)80143-8.

Shoham, O. 2006. *Mechanistic Modeling of Gas-Liquid Two-Phase Flow in Pipes*. Richardson, Texas, SPE.

Skopich, A. 2012. Experimental Study of Surfactant Effect on Liquid Loading in 2-in and 4-in Diameter Vertical Pipes. MSc thesis, University of Tulsa, Tulsa, OK.

Soedarmo, A., Fan, Y., Pereyra, E., and Sarica, C. 2018a. A Unit Cell Model for Gas-Liquid Pseudo-Slug Flow in Pipes. *Journal of Natural Gas Science and Engineering,* Vol. **60**, 125–143. https://doi.org/10.1016/j.jngse.2018.10.006.

Soedarmo, A., Pereyra, E., and Sarica, C. 2018b. A Simplified Model for Steady-State Pseudo-Slug Flow. Paper presented at the Offshore Technology Conference, Houston, Texas, USA. https://doi.org/10.4043/28996-MS.

Soedarmo, A., Soto-Cortes, G., Pereyra, E., Karami, H., and Sarica, C. 2018c. Analogous Behavior of Pseudo-Slug and Churn Flows in High Viscosity Liquid System and Upward Inclined Pipes. *International Journal of Multiphase Flow,* Vol. **103**, 61–77. https://doi.org/10.1016/j.ijmultiphaseflow.2018.02.001.

Soedarmo, A. 2019. Gas-Oil Flow in Upward-Inclined Pipes: Pseudo-Slug Flow Modeling and Upscaling Studies. PhD dissertation, University of Tulsa, Tulsa, OK.

Soleimani, A., Al-Sarkhi, A., and Hanratty, T.J. 2002. Effect of Drag-Reducing Polymers on Pseudo-Slugs – Interfacial Drag and Transition to Slug Flow. *International Journal of Multiphase Flow* **28** (12): 1911–1927. https://doi.org/10.1016/S0301-9322(02)00110-6.

Taitel, Y. and Dukler, A.E. 1976. A Model for Predicting Flow Regime Transitions in Horizontal and Near Horizontal Gas-Liquid Flow. *AIChE J* **22** (1): 47–55. https://doi.org/10.1002/aic.690220105.

Tang, H., Bailey, W., Stone, T., and Killough, J. 2019. A Unified Gas-Liquid Drift-Flux Model for Coupled Wellbore-Reservoir Simulation. Paper presented at the SPE Annual Technical Conference and Exhibition, Calgary, Alberta, Canada, September. https://doi.org/10.2118/195885-MS.

Taylor, N.S.H., Hewitt, I.J., Ockendon, J.R., and Witelski, T.P. 2014. A New Model for Disturbance Waves. *International Journal of Multiphase Flow,* Vol. **66**, 38–45. https://doi.org/10.1016/j.ijmultiphaseflow.2014.06.004.

Tengesdal, J. Ø., Kaya, A. S., and Sarica, C. 2019. Flow-Pattern Transition and Hydrodynamic Modeling of Churn Flow. *SPE J.,* Vol. **4**, 342-348. https://doi.org/10.2118/57756-PA.

Thaker, J. and Banerjee, J. 2015. Characterization of Two-Phase Slug Flow Sub-Regimes Using Flow Visualization. *Journal of Petroleum Science and Engineering* Vol. **135**, 561–576. https://doi.org/10.1016/j.petrol.2015.10.018.

Van der Meulen, G.P. 2012. Churn-Annular Gas-Liquid Flows in Large Diameter Vertical Pipes. PhD dissertation, University of Nottingham, Nottingham, United Kingdom.

Vaze, M.J. and Banerjee, J. 2011. Experimental Visualization of Two-Phase Flow Patterns and Transition from Stratified to Slug Flow.
Proceedings of the Institution of Mechanical Engineers, Part C: *Journal of Mechanical Engineering Science,* Vol. **225**, 382–389. https://doi.org/10.1243/09544062JMES2033

Wallis, G.B. 1969. *One-Dimensional Two-Phase Flow*. New York City: McGraw-Hill Book Company.

Wilkens, R. and Jepson, W.P. 1996. Studies Of Multiphase Flow in High Pressure Horizontal and+ 5 Degree Inclined Pipelines. Paper presented at the The Sixth International Offshore and Polar Engineering Conference, Los Angeles, California, USA.

Xiao, J.J., Shoham, O., and Brill, J.P. 1990. A Comprehensive Mechanistic Model for Two-Phase Flow in Pipelines. Paper presented at the SPE Annual Technical Conference and Exhibition, New Orleans, Louisiana. https://doi.org/10.2118/20631-MS.

Zabaras, G., Menon, R., Schoppa, W., and Wicks, M. III. 2013. Large Diameter Riser Laboratory Gas-Lift Tests. Paper presented at the Offshore Technology Conference, Houston, Texas, USA.

Zhang, H., Wang, Q., Sarica, C., and Brill, J. P. 2003. Unified Model for Gas-Liquid Pipe Flow via Slug Dynamics - Part 1: Model Development . ASME. *J. Energy Resour. Technol*. **125** (4): 266–273. https://doi.org/10.1115/1.1615246.

Zhu, Q. 2019 Intermittent Flow Analysis in Inclined Large Diameter Pipes. MSc thesis, University of Tulsa, Tulsa, OK.

Zuber, N. and Findlay, J.A. 1965. Average Volumetric Concentration in Two-Phase Flow Systems. *Journal of Heat Transfer* **87** (4): 453–468. https://doi.org/10.1115/1.3689137.

APPENDIX A

SUPPLEMENTAL FILES

A.1 Copyright Permissions

Permissions to include previously published materials in this thesis may be found in Supplemental File Figures_Permissions_Aljasser.pdf.